Development of Heterogeneous Catalysts for Methane Conversion and CO_2 Electroreduction

A Thesis

Submitted in partial fulfilment for the degree of

Master of Science

(as part of Integrated Ph.D. programme in Material Science)

By

Nijita Mathew

Chemistry and Physics of Materials Unit

JAWAHARLAL NEHRU CENTRE FOR ADVANCED SCIENTIFIC RESEARCH

(A Deemed University)

Bengaluru - 560064

March 2019

Dedicated to my family

DECLARATION

I hereby declare that the matter embodied in the thesis entitled "**Development of Heterogeneous Catalysts for Methane Conversion and CO_2 Electroreduction**" is the result of investigations carried out by me at the Chemistry and Physics of Materials Unit, Jawaharlal Nehru Centre for Advanced Scientific Research, India under the supervision of Prof. M. Eswaramoorthy and that it has not been submitted elsewhere for the award of any degree or diploma.

In keeping with the general practice in reporting the scientific observations, due acknowledgement has been made whenever the work described is based on the findings of other investigators. Any omission that might have occurred due to oversight or error in judgement is regretted.

Nijita Mathew

(Int. Ph.D. Student)

CERTIFICATE

I hereby certify that the work described in the thesis entitled **"Development of Heterogeneous Catalysts for Methane Conversion and CO_2 Electroreduction"** has been carried out by **Ms. Nijita Mathew** under my supervision at the Chemistry and Physics of Materials Unit, Jawaharlal Nehru Centre for Advanced Scientific Research, India, and that it has not been submitted elsewhere for the award of any degree or diploma.

Prof. M. Eswaramoorthy

(Research Supervisor)

ACKNOWLEDGEMENT

First and foremost, I express my sincere gratitude to Prof. M. Eswaramoorthy, my research supervisor, for his constant guidance throughout my M.S. thesis.

I express my sincere gratitude to Prof. C.N.R. Rao, FRS for being a constant source of inspiration and for creating an environment conducive for research.

I would like to thank my course work instructors Prof. S. Balasubramanian, Prof. Chandrabhas Narayan, Prof. Rajesh Ganapati, Prof. A. Sundaresan, Prof. Shobhana Narasimhan, Prof. Ranjan Dutta, Prof. U. V. Waghmare, Prof. Swapan K. Pati, Prof. Kanishka Biswas, Prof. Sebastian C. Peter, Dr. Premkumar Senguttuvan, Dr. Sarit Agasti, Prof. Aloknath Chakraborty (IISc), Prof. N. Ravishankar (IISc), Prof. Sridhar Rajaram, Prof. K.S. Narayan for their wonderful and enriching classes.

I express my heartfelt gratitude to Momin and Soumita for their help, support and guidance in carrying out my experiments and for helping in completing my thesis on time.

I would like to thank my present and former labmates Sonu, Suchi, Divya, Arunava, Surishi, Abhishek, Dr. Mehraj, Dr. Shivanna, Dr. Dheeraj, Dr. Sisir, Dr. Sushumna, Dr. Monoj, Subramanya, Bibekannanda, Himani, Doha, Anusha and Kapil (winter intern) for all their support, guidance and for creating a friendly and stress free lab environment.

I thank all the technical staff at JNCASR. My sincere thanks go to Mr. Vasu, Mr. Anil, Mrs. Usha, Mrs. Selvi, Mr Kannan and Mr Rahul for their timely help in carrying out various characterizations.

I am also thankful to all academic, administrative, security, Dhanvantri, library and comp lab staff for making life in JNCASR easy.

I would like to thank my Integrated Ph.D. batchmates Shashank, Ashutosh, Pragya, Raagya, Brijesh and Tarandeep for all their support and for making my hostel life enjoyable.

I would further like to thank all my friends at JNCASR who were a good company and made each day in hostel enjoyable.

Above all, I thank my relatives, grandparents, parents and my brother, for believing in me and for standing by me in all my endeavours. Without them it would have been impossible to achieve my goals. I dedicate my thesis to my family.

Finally, I thank God almighty for giving me strength to face all the situations that came in my way and for giving me hope when I lost it.

CONTENTS

Chapter 3: Electrochemical CO_2 reduction

PREFACE

This thesis deals with the development of heterogeneous catalyst for methane conversion via non- oxidative coupling and electrochemical CO_2 reduction. It is known that the gases like methane and carbon dioxide contribute towards global warming. Hence there is requirement of efficient methods to mitigate the excess presence of these gases in the atmosphere. In this thesis efforts have been put in to develop heterogeneous catalyst towards this cause.

Chapter 1 gives a brief introduction into catalysis. The chemistry behind the catalytic activity over a solid surface have been briefly discussed. Furthermore, different synthesis strategy and the causes of catalyst deactivation have been discussed.

Chapter 2 deals with hydrothermal synthesis of Pt-Sn bimetallic system supported on ZSM-5. Pt based systems are known to be efficient for methane activation. However, it undergoes deactivation with time due to coke deposition. Addition of Sn, increases the electron density which makes the catalyst coke resistant.

Chapter 3 deals with synthesis of Pd supported on g-C_3N_4 for electrochemical reduction of carbon dioxide. Pd based system is known for the conversion of CO_2 to CO under high reduction potential. Pd have been dispersed over g-C_3N_4 which is electrochemically active due to the presence of triazine units.

Chapter-1

Introduction

Catalysis have been a part of the human civilization since centuries. One of the early examples of catalysis is the fermentation of biological materials such as grapes, rice, etc to produce ethyl alcohol using yeast. However, the concept of catalysis was formulated much later. It was in 1835 that J.J. Berzelius coined the term catalysis based on the conclusions he drew from the experiments of the contemporary scientists. Based on his observations, he proposed the following [1]:

"It is then shown that several simple and compound bodies, soluble and insoluble, have the property of exercising on other bodies and action very different from chemical affinity. The body affecting the changes does not take part in the reaction and remains unaltered through the reaction. This unknown body acts by means of an internal force, whose nature is unknown to us. This new force, up till now unknown, is common to organic and inorganic nature. I do not believe that this force is independent of the electrochemical affinities of matter; I believe on the contrary, that it is a new manifestation of the same, but, since we cannot see their connection and independence, it will be more convenient to designate the force by a new name. I will, therefore, call it the "Catalytic Force," and I will call "Catalysis" the decomposition of bodies by this force, in the same way, that we call by "Analysis" the decomposition of bodies by chemical affinity."[1]

These words marked the beginning of research in the field of catalysis. A catalyst is hence defined as the substance that accelerates the attainment of equilibrium of a thermodynamically feasible chemical reaction by providing an alternative minimum energy pathway without itself undergoing any permanent chemical change. Several catalyst have been studied and many of them have been commercialized for the production of several value-added chemicals.

Some of the early industrial catalytic processes involves Haber-Bosch process for ammonia synthesis which is an essential feedstock for fertilizer industry, Fischer-Tropsch process for hydrocarbon synthesis and steam reforming of hydrocarbons for the generation of syngas ($CO+H_2$) which is a precursor for synthesis of many chemicals. These commercialized processes have certain disadvantages. Firstly, the requirement of extreme conditions such as high pressure or high temperature and production of large amount of unwanted by-products makes these processes non-economical. Secondly, harmful gases released pollutes the environment and thereby contributes to the

greenhouse effect. The present-day research into catalysis thus focuses on development of catalyst and catalytic processes that is not only eco-friendly but is also cost-effective.

1.1. Types of Catalysis

Catalysis is further subdivided into heterogeneous, homogeneous and biocatalysis.

1.1.1 Homogeneous Catalysis

In homogeneous catalysis, the catalysts, reactant and the products are in the same phase. The reaction is faster and is highly selective towards the desired product. The reaction generally proceeds by complex formation with the reactant molecules which is soluble in the reaction medium. An example of homogenous catalysis is the conversion of methane to methanol on Periana catalyst [2]. However, such catalytic reaction requires efficient separation of the product formed from the reaction medium which is difficult and adds to the cost.

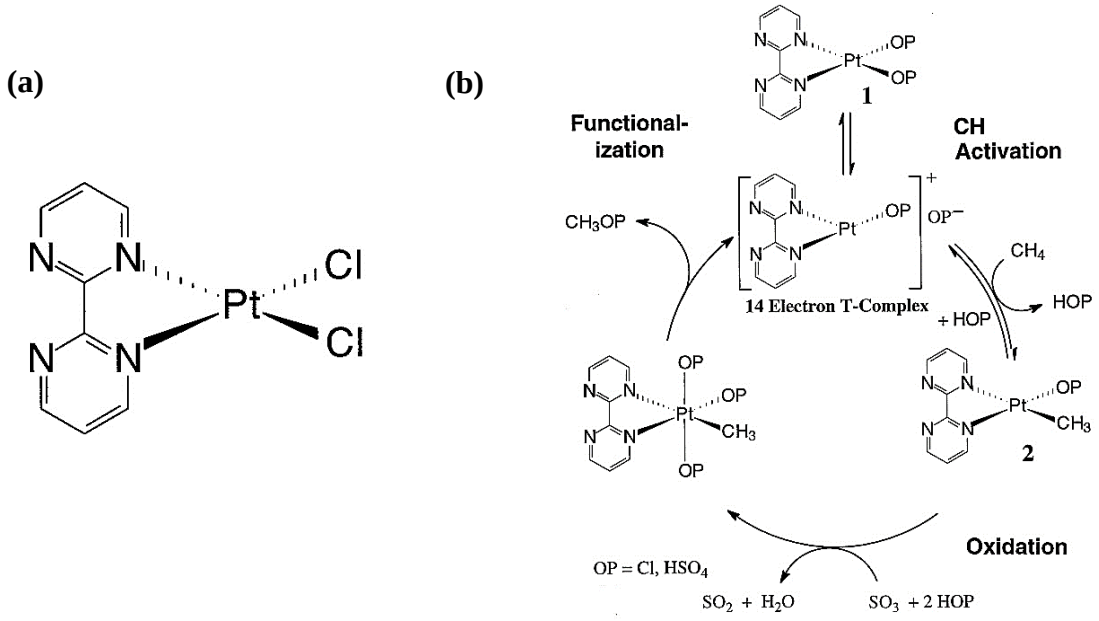

Figure 1: (a) *Periana catalyst,* **(b)** *Mechanistic pathway for the oxidation of methane to methanol (reprinted with permission from ref. 2).*

1.1.2 Heterogeneous Catalysis

In heterogeneous catalysis, the catalyst, reactants and the products are in different phases. The reaction generally proceeds by the adsorption of the reactant molecule on the catalyst surface. An example of heterogeneous catalysis is the Haber-Bosch process, where the catalyst i.e. Fe is in the solid state while the reactants H_2 and N_2 are in the gaseous phase. The rate of the reaction is slower and many unwanted by-products are formed in the heterogeneous catalytic reactions. However, the separation of the desired product from the reaction chamber is easier compared to homogenous catalysis.

Heterogeneous catalysis can be subdivided into electrocatalysis, photocatalysis and thermocatalysis based on the type of catalyst employed. Electrocatalysis and photocatalysis today is receiving greater attention as development of such technologies would not only be environment friendly but will also be economically viable.

1.1.3 Biocatalysis

In bio-catalysis, enzymes act as the catalyst. Enzymes are large proteins. They are highly specific. The active sites present on these enzymes have different shapes. The substrate molecule that has the same geometric shape, as the active site, only can bind to the enzyme. This results in an enzyme-substrate complex which later dissociates to give the product and the active site is free for further reaction. This is known as lock and key mechanism as shown in figure 2. This type of mechanistic pathway makes biocatalysis highly specific and efficient. An example of biocatalysis is the decomposition of hydrogen peroxide to water and oxygen by the enzyme catalase.

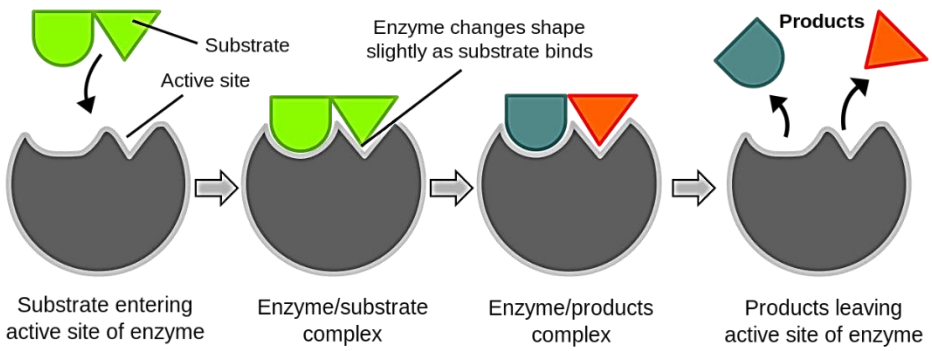

Figure 2: *Lock and key mechanism observed in biocatalysis (adapted from ref.3)*

1.2 Chemistry behind Catalytic Reactions

Chemical kinetics govern the chemistry behind the catalytic reactions. An understanding of the kinetics of the catalytic reaction gives mechanistic insight which helps in the development of more eco-friendly and cost-effective industrial processes. It thus links the reaction dynamics with the physical parameters such as the temperature and the pressure. The rate of a reaction is given by the rate law. For a reaction A→B, the reaction rate equation is given as:

$$\mathbf{Rate = k[A]^x}$$

Here k stands for the reaction rate constant, [A] is the concentration of reactant A and x is the order of the reaction. The rate constant, k is not a true constant as it depends on temperature. In 1903, Noble laureate Svante August Arrhenius formulated the relationship between temperature and rate constant as the Arrhenius equation:

$$\mathbf{k = Ae^{-Ea/RT}}$$

Here A is the pre-exponential factor, E_a is the activation energy, R is the universal gas constant and T is the temperature.

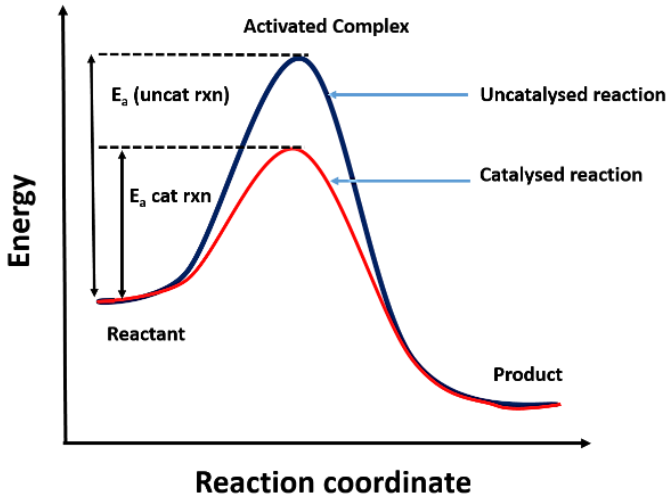

Figure 3: *Energy profile of a catalytic reaction*

For a reaction to proceed, it must overcome the energy barrier (Fig 3). The activation energy is thus an important parameter as it is a measure of the minimum amount of energy

required to overcome the energy barrier for the reaction to proceed. Higher the activation energy, slower will be the rate of the reaction. The rate of the reaction is found to double with every 10 ^{o}C rise in temperature.

A catalytic reaction takes place only when the reacting species comes in contact with the catalyst. Both physisorption and chemisorption plays a role in the catalytic processes. Physisorption is mainly governed by van der waals interaction between the adsorbent and the adsorbate as a result the reacting species are weakly adsorbed over the catalyst surface. Physisorption does not involve any significant change in activation energy and thus it is a faster process. On the contrary, the reacting species are covalently bonded to the catalyst surface in chemisorption. As a result, the activation energy plays a key role in governing the rate of the reaction. Hence, chemisorption is slower and is also known as activated adsorption.

The adsorption of the reacting species on to a solid surface take place at certain sites only. These sites are known as the active sites of the catalyst. Studies into the solid surface have revealed that on a solid surface, there are three kinds of site where the atom resides namely, terrace site, step site, kink site and adatom, (which projects out of the surface) as shown in figure 4.

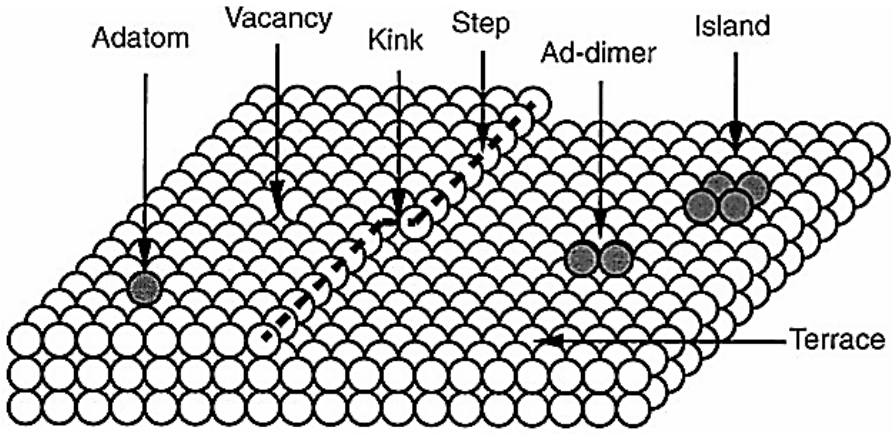

Figure 4: *Different sites on a solid surface. (taken from ref 4.)*

These sites have different properties which affect the atom distribution, chemisorption, mechanistic pathway and thereby the rate of a reaction. For example, Somerjai *et al.* have shown that Pt surface has three faces (-111), (-557) and (-679). The atom distribution varies on these faces. Maximum number of Pt atoms reside on the terrace and step sites

corresponding to (-111) face. While the (-679) face has more kinks and less number of platinum atoms reside on these sites [5]. Thus terrace sites are found to be catalytically more active. Further, in case of chemisorption, the reaction takes place between the adsorbed species. The rate of the reaction varies on different sites of the catalyst. The faces which have more number of active site will have less activation energy and thereby the reaction will be faster. Hence, the overall rate of a reaction would be the sum of the rate of reaction at different sites. Examples of bimolecular reactions that take place on the solid surface are mentioned in the following section.[6]

1.3 Mechanism for bimolecular reactions

Three different mechanistic pathways have been proposed for the bimolecular reaction in case of heterogeneous catalysis namely:

1. Langmuir-Hinshelwood Mechanism
2. Eley-Rideal Mechanism
3. Mars-Van Krevelen Mechanism

1.3.1 Langmuir Hinshelwood Mechanism

According to this mechanism, all the reactant species are first adsorbed on the surface of the catalyst [3, 22]. The adsorbed species are in thermal equilibrium with the surface. The reaction between the adsorbed species takes place on the surface as shown in figure 5. p-Nitrophenol reduction to aminophenol by sodium borohydride in the presence of a metal catalyst is a typical example of this mechanism. During the reduction reaction over a metal nanoparticle, nitrophenol and BH_4^- gets adsorbed over the metal surface. The adsorbed species then undergo reaction to form aminophenol [7]. Other examples which follows similar mechanism are Mn containing oxides for SCR of NO_x in presence of NH_3 [8], reduction of 2-nitroaniline on Au nanoparticles [9].

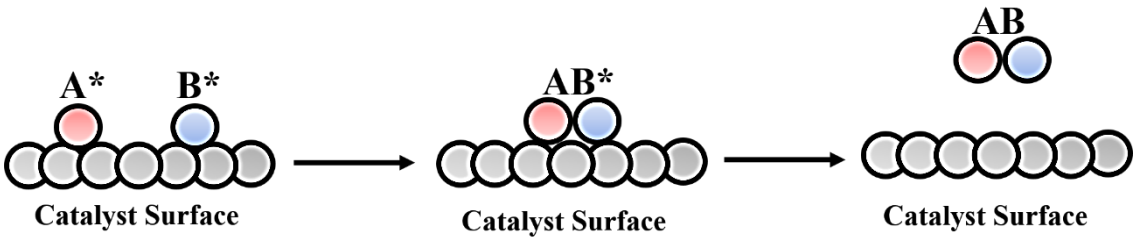

Figure 5: *Schematics for Langmuir- Hinshelwood kinetics.*

1.3.2 Eley-Rideal Mechanism

In this mechanism, one of the reacting species completely covers the catalyst surface initially to form a monolayer, and the second specie reacts directly from the gas phase without adsorbing onto the catalyst surface to form the product as shown in the schematic in figure 6.

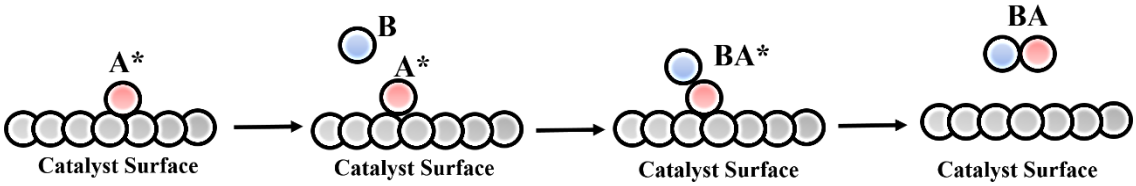

Figure 6: S*chematics for Eley-Rideal kinetics.*

An example of this mechanism is observed in the catalytic CO oxidation observed over single Pt atom supported on N-doped graphene for CO oxidation [10]. Theoretical calculations showed that it follows a tri-molecular Eley-Rideal mechanism wherein CO completely occupies the active Pt sites of the catalyst initially. This is followed by the reaction with oxygen. During the reaction the oxygen molecule simultaneously interacts with two surface adsorbed CO molecule. This results in the elongation of O-O bond and the formation of OCO-OCO intermediate. Subsequently, the CO_2 formed desorbs from the surface.

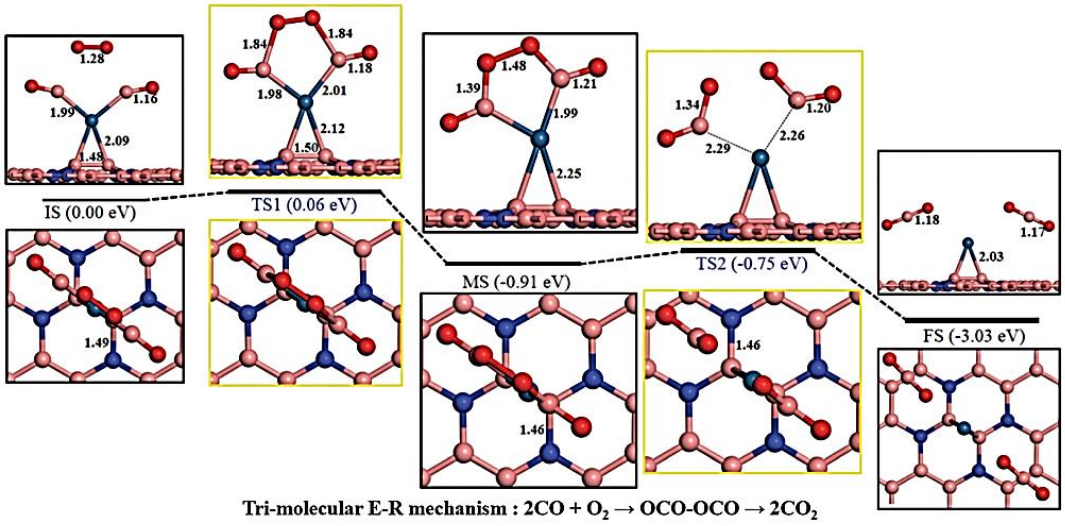

Figure 7: *Tri molecular Eley-Rideal mechanism for CO oxidation observed over Pt supported on N-doped graphene. (printed with permission from ref 10).*

1.3.3 Mars-Van Krevelen Mechanism

In this mechanism, adsorption of one reacting molecule takes place over the pre-adsorbed reacting molecule to form the reaction intermediate that remains adsorbed. This intermediate then gets converted to the product which is then desorbed from the surface. A vacancy is created by desorption of the product formed. The vacant site is then occupied by the reactant molecule.

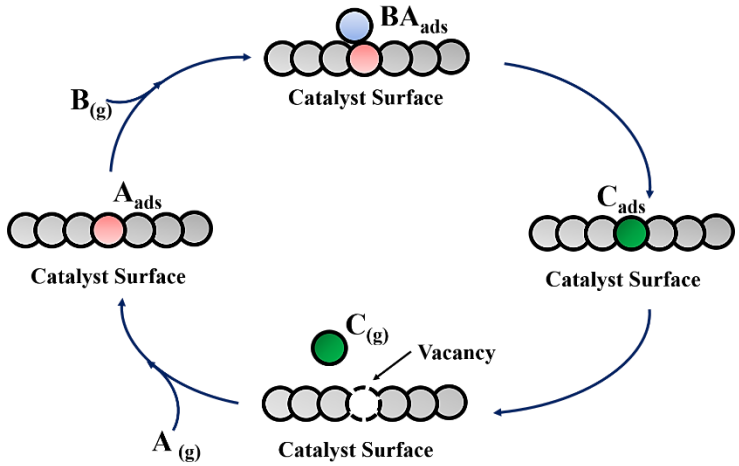

Figure 8: S*chematics for Mars-Van Krevelen mechanism.*

An example of this mechanism is CO hydrogenation on iron carbide [11]. Theoretical calculations show that hydrogenation of carbides results in the formation of methyl

species at the bridge position between the Fe atoms. Adsorption of CO displaces the methyl species to the adjacent carbide atom.

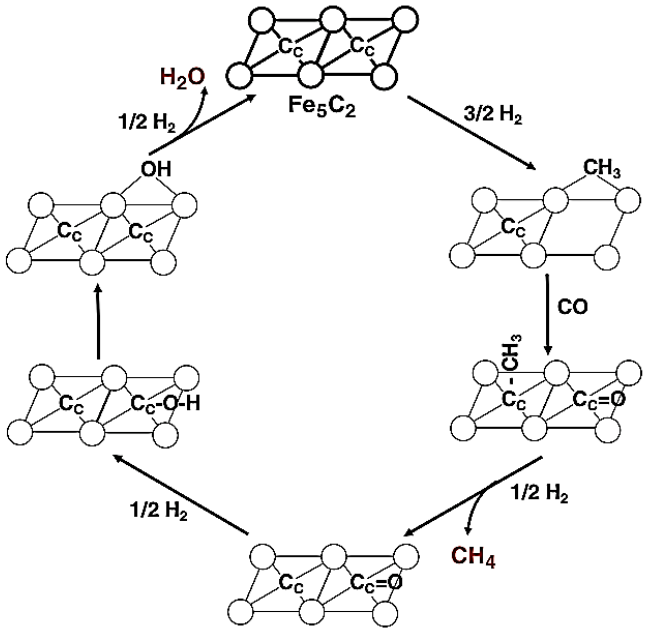

Figure 9: *Mars Van Krevelen mechanism observed for hydrogenation of CO over iron carbide. (printed with permission from ref 11)*

1.4 Preparation of Catalyst

The heterogeneous catalysis takes place on the surface (or within the pores) of the catalyst and hence the catalyst synthesised must have a high active surface area. To ensure high catalytic activity, different catalyst supports are used such as the oxides, nitrides, sulphides etc. Table 1 gives some of the most commonly used oxide based supports and their nature. The active component of the catalysts are dispersed over these supports. A well dispersed catalyst further ensures that all the active components responsible for catalysis are well exposed and are easily accessible to the reactant molecules. This ensures, effective collision and adsorption. Hence increasing the rate of the reaction.

Table 1: *Types of metal oxides commonly used and their melting points (adapted from ref. 12)*

S. No.	Oxide	Melting point (K)	Oxide type
1.	γ- Al_2O_3	2318	Acidic
2.	α- Al_2O_3	2318	Amphoteric
3.	SiO_2	1973	Acidic
4.	SiO_2- Al_2O_3	1818	Very acidic
5.	MgO	3073	Basic

1.4.1 Impregnation

This method depends on the interaction between the porous support and the metal precursor present in the solution. Precursors commonly used are inorganic metal salts such as the metal nitrates, sulfates, chlorides etc. Water is the most commonly used solvent because of the high solubility of most of the metal salts in it. The added component may be present on the surface of the support or it may be taken up by capillary action into the pores of the catalyst. The ions present on the surface of the support are not as stable as those present within the pores. These may be washed away during catalyst preparation or may lead to catalyst deactivation by sintering. Impregnation is of two types: wet impregnation and incipient wetness impregnation. [13]

In case of wet impregnation an excess amount of precursor solution is used. This ensures that sufficient ions are present which could be taken up by the support. However, it is difficult to control the weight of the added component taken up by the support. In case of incipient wetness impregnation or dry impregnation, the amount of precursor solution taken is just enough to fill the pore volume of the support taken. The advantage of this method is that the weight of the added metal ions can be controlled. However, it is difficult to ensure uniform distribution of the added component.

1.4.2 Coprecipitation

Here the catalyst support and the metal precursor is dissolved in a common solvent. The resultant solutions are mixed. The support and the active metal ions combine and precipitate out. The nucleation and growth is affected by the temperature, pH, and

concentration of the ions in the solution and solubility of the combined solid precursor. This method is suitable for obtaining high metal loading in a catalyst. An example of this is the coprecipitation of NiO and ZrO_2 to obtain high weight percent loading of metal ions. [14]

1.4.3 Solvothermal method

In this method, a saturated precursor solution is heated inside a sealed autoclave above its boiling point. The autogenous pressure developed inside the autoclave due to the vapour pressure of the solvent is responsible for the nucleation and growth of the crystal. Further aging of the crystals thus formed results in the formation of the desired nanostructure. Synthesis of Sn-modified ZSM-5 is an example of this method [15].

Apart from the conventional methods of catalyst preparation, there are several other non-conventional methods such as microwave assisted synthesis and electrodeposition are extensively used. These methods are well known as they help in faster catalyst preparations.

1.4.4 Microwave synthesis

Microwave assisted synthesis has received attention because of faster reaction rates and use of environmentally benign solvents. Microwave flash heating induces rapid rotation of the reactant molecules which generates sufficient heat due to friction. The heat generated helps in overcoming the reaction energy barrier and thereby enhances the rate of the reaction. As the reaction is faster compared to the conventional techniques, the reactant molecules do not stay at higher temperature for a long time which prevents it from decomposition [16].

1.4.5 Electrodeposition

This is an electrochemical method which is used in the preparation of electrocatalyst. The electrocatalyst must be coated onto an appropriate conducting substrate like the carbon paper to study an electrochemical reaction. Binders like nafion are added to coat the electrocatalyst onto the substrate. Using binders may block the catalytically active sites and may therefore reduce the catalytic activity. Hence binder free techniques like electrodeposition are employed wherein the metal catalyst is directly deposited on to the

substrate [10]. Synthesis of an electrocatalyst by this method is faster. It consists of multiple steps [7, 20, 21]: (1) diffusion of the ion to the electrode surface, (2) electron transfer, (3) surface diffusion of the adsorbed atoms, (4) nucleation and growth as shown above in Figure 10. Employing this synthesis strategy is advantageous because the morphology, thickness and composition of the catalyst can be controlled by varying the electrolyte and the applied potential [10].

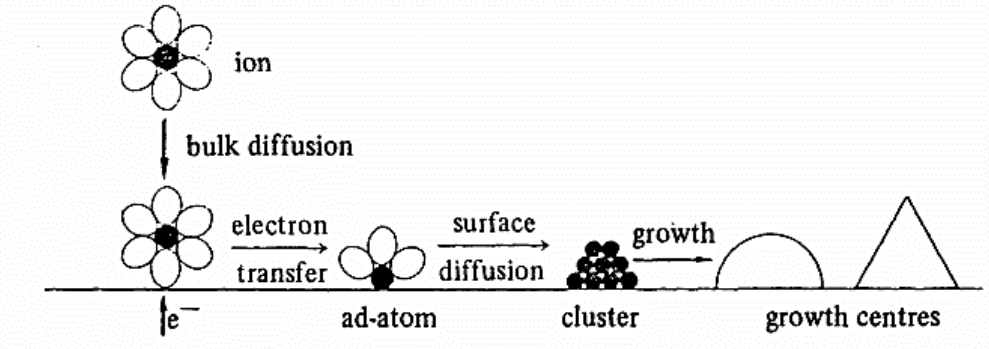

Figure 10: *Steps involved in electrodeposition of a metal on a substrate. (printed with permission from Ref.7)*

1.5 Catalyst Deactivation

Deactivation of the catalyst is a very common phenomenon wherein the catalyst becomes less active as the reaction progresses. There are several means by which a catalyst gets deactivated such as sintering, catalyst poisoning, and catalyst inhibition. [17]

1.5.1 Sintering

This is a kind of thermal degradation of the catalyst. This can happen by atom migration, crystallite migration or when the catalyst structure collapses. In case of atom migration, the metal atoms moves from one crystallite to another crystallite either through the surface of the catalyst or through the gas phase. Thus the smaller clusters become smaller, and the bigger clusters become bigger in size. This results in the decrease of the number of active sites.

In case of crystallite migration, the crystallite itself migrates, collides and coalesce with other crystallites which leads to bigger clusters and hence the number of active sites exposed to the reactant decreases. However, at higher temperatures, sintering takes place

when the catalyst support collapse. This blocks the pores leading to the active site. As a result, the active sites becomes inaccessible to the substrate molecules. Sintering is affected by several other factors such as the temperature, atmosphere, metal involved, support, promoter etc. [18]

1.5.2 Catalyst Poisoning

Strong chemisorption of the reactants, products and the impurities on the active site of the catalyst is known as the catalyst poisoning. Some of the well-known catalyst poisons include organic bases, carbon, compounds of sulphur, phosphorus etc.

Poisoning can be of two types, selective and non-selective. Selective poisoning refers to the preferential adsorption of the poisoning molecule only to specific active sites of the catalyst. For example, the CO poisoning of the nickel-based catalyst involved in the exchange of hydrogen atoms on the benzene ring of para-xylene [19]. Nonselective poisoning refers to the binding of the poisoning molecules to all the active sites of the catalyst without any preference. For example, the binding of the phosphorus to the active site of the automotive catalyst [18]. The catalyst poisoning is said to be reversible if the catalyst can be regenerated, while it is irreversible if the molecule is bound very strongly to the active site and the catalyst cannot be regenerated.

1.6 Conclusion

The increase in the demand of value-added chemicals owing to the ever increasing population and the continuously deteriorating environmental condition requires further innovations in the existing catalysts based technology. This will not only help in meeting the existing demands but will also help in reducing the waste products and making the industrial processes more eco-friendly. In the present work, efforts have been made to develop catalyst by both conventional and non-conventional method. The catalysts prepared is used to study non –oxidative coupling of methane and CO_2 electroreduction.

1.7 References

1. Lindström, B.; Pettersson, L. J. A Brief History of Catalysis. *Cattech,* **2003**, *7* (4), 130–138.

2. Periana, R. A.; Taube, D. J.; Gamble, S.; Taube, H.; Satoh, T.; Fujii, H. Platinum Catalysts for the High-Yield Oxidation of Methane to a Methanol Derivative. *Science*, **1998**, *280*.

3. https://simple.wikipedia.org/wiki/Enzyme#/media/File:Induced_fit_diagram.svg

4. https://slideplayer.com/slide/7508829/

5. Kesmodel, L. L.; Somorjai, G. A. Structure of Solid Surfaces. *Acc. Chem. Res.* **1975**, *I* (4), 392–398.

6. Keith J. Laidler, *Chemical kinetics*, 4th edition, Pearson Education, **2007.**

7. Southampton Electrochemistry Group, *Instrumental methods in electrochemistry*, WP ltd., **2011.**

8. Zhang, S.; Zhang, B.; Liu, B.; Sun, S. A Review of Mn-Containing Oxide Catalysts for Low-Temperature Selective Catalytic Reduction of NO_x with NH_3: Reaction Mechanism and Catalyst Deactivation. *RSC Adv.* **2017**, *7* (42), 26226–26242.

9. Naeem, H.; Ajmal, M.; Muntha, S.; Ambreen, J.; Siddiq, M. Synthesis and Characterization of Graphene Oxide Sheets Integrated with Gold Nanoparticles and Their Applications to Adsorptive Removal and Catalytic Reduction of Water Contaminants. *RSC Adv.* **2018**, *8* (7), 3599–3610.

10. Xilin Zhang, Zhansheng Lu, Guoliang Xu, Tianxing Wang, Dongwei M, C.; Yang, Z. Y. and L. Single Pt Atom Stabilized on Nitrogen-Doped Graphene : CO Oxidation Readily Occurs via The. *Phys. Chem. Chem. Phys.* **2015**, 20006–20013.

11. Gracia, J. M.; Prinsloo, F. F.; Niemantsverdriet, J. W. Mars-van Krevelen-like Mechanism of CO Hydrogenation on an Iron Carbide Surface. *Catal. Letters* **2009**, *133* (3–4), 257–261.

12. Julian R.H. Ross, *Heterogenous Catalysis fundamentals and applications* (Elsevier, 2012).

13. Munnik, P.; De Jongh, P. E.; De Jong, K. P. Recent Developments in the Synthesis of Supported Catalysts. *Chem. Rev.* **2015**, *115* (14), 6687–6718.

14. Spinner, N.; Mustain, W. E. Electrochemical Methane Activation and Conversion to Oxygenates at Room Temperature. *J. Electrochem. Soc.* **2013**, *160* (11), F1275–F1281.

15. Yang, X.; Wang, F.; Wei, R.; Li, S.; Wu, Y.; Shen, P.; Wang, H.; Gao, L.; Xiao, G. Synergy Effect between Hierarchical Structured and Sn-Modified H[Sn, Al]ZSM-5 Zeolites on the Catalysts for Glycerol Aromatization. *Microporous Mesoporous Mater.* **2018**, *257*, 154–161.

16. Polshettiwar, V; Varma, R.S., *Aqueous Microwave Assisted Chemistry- Synthesis and Catalysis*, RSC, **2010.**

17. Gadi Rothenberg, *Catalysis concepts and green applications*, (Wiley-VCH, 2008).

18. Bartholomew, C. H. Mechanism of Catalyst Deactivation. *Appl. Catal. A Gen.* **2001**, *212*, 17–60.

19. M. J. Philips, E. Crawford, C. K. Selective Poisoning of Catalytic Activity. *Nature* **1963**, 487.

20. Bruno, T. J. Laboratory Scale Electrodepositon: Practice and Applications. *J. Chem. Educ.* **2009**, *63* (10), 883.

21. Mohanty, U. S. Electrodeposition: A Versatile and Inexpensive Tool for the Synthesis of Nanoparticles, Nanorods, Nanowires, and Nanoclusters of Metals. *J. Appl. Electrochem.* **2011**, *41* (3), 257–270.

22. Mironenko, A. V.; Vlachos, D. G. Conjugation-Driven "Reverse Mars-van Krevelen"-Type Radical Mechanism for Low-Temperature C-O Bond Activation. *J. Am. Chem. Soc.* **2016**, *138* (26), 8104–8113.

23. I. Chorkendorff, J.W. Niemantsverdriet, *Concepts of Modern Catalysis and Kinetics*, (Wiley-VCH, 2007).

24. J.M. Thomas, W.J. Thomas, *Principles and Practice of Heterogenous Catalysis*, (VCH, 2008).

Chapter 2

Non-Oxidative Coupling of Methane

2.1 Introduction

Natural gas is an abundant and clean fossil energy source. With depleting oil reserves, it has received greater attention to meet the global energy demand. Extraction and processing of natural gas has thus increased over the years. However, this process has resulted in the emission of methane. This is one of the biggest concern today because methane is a more potent greenhouse gas compared to CO_2 and over the next hundred years, it is expected to cause severe damage to the environment. Hence, there is a need to find an environment friendly solution to this rising concern.

Further motivation to find a solution to mitigate the excess methane released stems from three main factors. Firstly, a large amount of methane emitted onsite could not be captured and is usually flared up during the extraction process which results in the loss of a large amount of hydrocarbon feedstock. Secondly, the methane reserves are located in remote areas and hence has to be transported over a long distance to be put into further use. Further, conversion of methane to value added chemicals proceeds via a two-step process, wherein methane is first converted to syn gas before being transformed into any value added chemicals. This two-step process is highly energy intensive. Hence, development of an economically viable and environmental friendly onsite technology to utilise the methane emitted is necessary [5].

Methane can be directly converted to some of the essential building blocks of the chemical industry such as small hydrocarbons like ethylene, propylene or aromatic molecules like benzene, naphthalene etc. Research into efficient conversion of methane have focussed on four major routes which are as follows:

1. **Dry Reforming of methane**

$$CH_4 + CO_2 \xrightarrow[\triangle]{\text{Catalyst}} CO + 2H_2 \qquad \Delta H = 247.3 \text{ kJ/mol } [1]$$

Dry reforming of methane helps in mitigating CO_2 along with methane. Despite being an efficient process, it suffers from various disadvantages such as coke deposition which leads to catalyst deactivation and high operating temperatures which makes this process energy intensive [2].

2. **Steam reforming of methane**

$$CH_4 + H_2O \xrightarrow[\triangle]{\text{Catalyst}} CO + 3H_2 \qquad \Delta H = 206 \text{ kJ/mol } [1]$$

Steam reforming is an industrially established process for syn gas production. The current challenges faced in this process is that it is a highly energy intensive process. Secondly, the production of hydrogen cannot be increased as the catalyst becomes unstable and has to be replaced at the regular intervals [3, 4].

3. **Oxidative coupling of methane**

$$CH_4 + 0.5O_2 \xrightarrow[\triangle]{\text{Catalyst}} C_2H_6 + H_2O \qquad \Delta H = -42.4 \text{ kJ/mol } [1]$$

$$CH_4 + O_2 \xrightarrow[\triangle]{\text{Catalyst}} C_2H_4 + 2H_2O \qquad \Delta H = -67.4 \text{ kJ/mol } [1]$$

This process deals with direct conversion of methane to hydrocarbon in the presence of oxidants such as O_2, SO_2, N_2O and CO_2. Despite being a promising method, it is not commercialised because the selectivity is very low due to over-oxidation of methane to carbon dioxide in the presence of the oxidants.

4. **Non oxidative coupling of methane (NOCM)**

$$2CH_4 \xrightarrow[\triangle]{\text{Catalyst}} C_2H_6 + H_2 \qquad \Delta H = 64.4 \text{ kJ/mol } [1]$$

$$2CH_4 \xrightarrow[\triangle]{\text{Catalyst}} C_2H_4 + 2H_2 \qquad \Delta H = 201.5 \text{ kJ/mol } [1]$$

Non oxidative coupling of methane (NOCM) on the other hand does not require oxygen and hence over-oxidation can be prevented. Secondly, it takes place at a lower temperature compared to dry reforming and steam reforming. However, the major challenge faced here is the rapid coke deposition that deactivates the catalyst easily. Hence, development of an efficient catalyst could make this process a promising technology for tomorrow.

Various thermochemical properties of methane are responsible for the high stability of the molecule. This has made the direct conversion of methane to hydrocarbon a challenge. The properties of methane is summarized in Table 1.

Table 1: *Properties of methane (adapted from ref. 5)*

S.No.	Property	
1.	Geometry	Tetrahedral
2.	Hybridization	sp^3
3.	C-H bond length	1.087 A^o
4.	H-C-H bond angle	109.5^O
5.	Polarizability	$2.84x\ 10^{-40}\ C^2\ m^2J^{-1}$
6.	Bond Dissociation Energy	439.3 kJ mol^{-1}
7.	Ionization Potential	12.6 eV
8.	Electron Affinity	-1.9 eV

The first step towards direct conversion of methane to hydrocarbon through methane coupling is the activation of methane which is the rate determining step wherein hydrogen is abstracted to get methyl radical, anion or a cation. The methyl group formed is responsible for further reaction. Methane activation is a slow step due to the high bond dissociation energy (table 1) of methane. Secondly, since all the four bonds of methane are equivalent, dipole moment of the molecule is negligible and hence the bonds are not polarised. Difficulty in methane activation can be further understood in terms of molecular orbitals [6, 7]. It has been observed that the HOMO –LUMO gap in an unreacted methane molecule is high which makes the reaction difficult. However, the HOMO-LUMO gap is altered upon interaction with the catalyst surface due to the distortion of the tetrahedral geometry which lowers the symmetry of the molecule and thereby facilitates the reaction.

Literature survey into non-oxidative coupling of methane reveals that the reaction takes place on catalysts which are acidic in nature. One of the most commonly used acidic support for NOCM are zeolites which are known as solid superacid [5]. Deprotonation and hydrogen exchange of methane are known to be catalyzed by the Brønsted acid sites present in these zeolites.

ZSM-5 based catalyst have been extensively studied for NOCM. It has received attention because of it porous structure and presence of large number of Brønsted acid sites which

will not only activate methane but will also increase the selectivity of the product formed. In ZSM-5, some of the silicon in the silica matrix are replaced by the Al^{3+} ion which is a low valence dopant. The doping with Al^{3+} ion results in an electron deficient region around the surrounding oxygen atoms within the framework [8]. In order to overcome the electron deficiency, the oxygen gets protonated. The hydroxyl group thus formed governs the acidity of the zeolite [9]. A zeolite is said to be less acidic if the O-H bond strength is high. The hydroxyl groups interact with the approaching methane molecule. This interaction lowers the tetrahedral symmetry of the molecule which makes methane activation feasible. The dehydrogenation and H-exchange takes place simultaneously on the Brønsted acid sites.

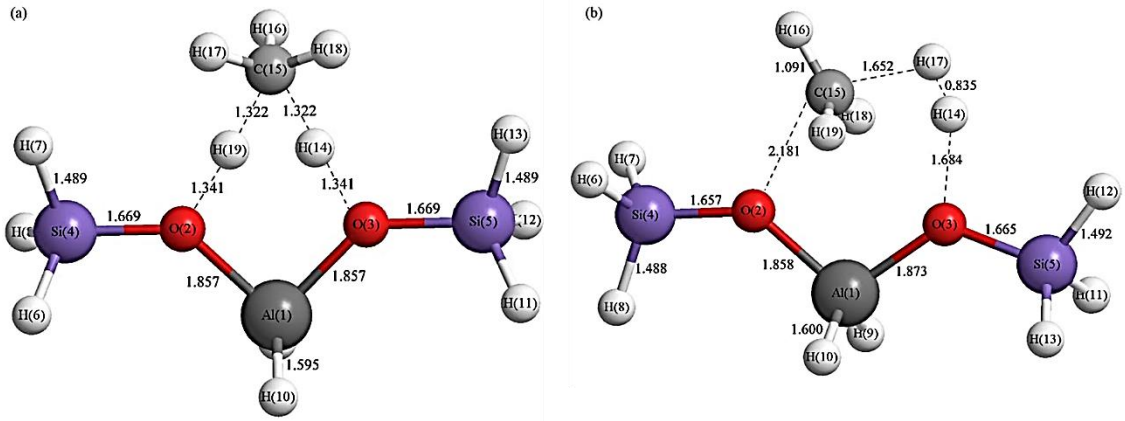

Figure 1: *Interaction of methane with framework oxygen in a zeolite and the corresponding transition state* **(a)** *hydrogen exchange reaction* **(b)** *dehydrogenation reaction. Color code: blue-Si, dark grey- Al, red- O, white- H, light grey- C. (taken with permission from ref. 10)*

Methane interacts with the hydroxyl group (as shown in Figure 1) and results in the formation of CH_5^+ intermediate wherein methane coordinates with the hydroxyl group and the coordinatively unsaturated site (i.e. framework oxygen atom). The framework oxygen atom acts as a Brønsted base by abstracting proton from methane. The CH_5^+ intermediate thus formed dissociates to form CH_3^+ and H_2 is released during the process [8]. Gas phase reaction of CH_3^+ with methane have established the formation of intermediates such as the $C_2H_7^+$ which ultimately breaks down to give ethylene (as shown in scheme1). However, conversion of methane on pure ZSM-5 is found to be very low.

Scheme 1: *Interaction of methane with the Brønsted acid sites (adapted from ref. 8)*

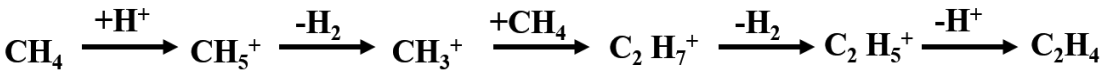

Modifying the zeolite by incorporation of transition metals have proven to increase the conversion and selectivity of the product formed. Pt [11, 12], Mo [13, 14, 15] and Fe [16, 17, 18] based catalyst have been explored for non-oxidative coupling of methane. Fe/SiO_2 showed a 40% conversion of methane with ~ 90% selectivity towards ethylene at 1363K [18]. Mo_2C/[B]ZSM-5 [19] showed a 2.4% conversion at 923K with 90% selectivity for ethylene. Although the selectivity for ethylene is good but the reaction temperature is quite high in case of Fe/SiO_2. In case of Mo_2C/[B]ZSM-5, the conversion is low and the catalyst gets deactivated very fast. Hence, there is a scope for further improvement in terms of catalyst stability and reaction temperature.

Conversion of methane to higher hydrocarbon over Pt based system was first reported in 1991, wherein the selectivity of C_2 hydrocarbon was found to be 60% over EUROPT-1 [41] ($Pt@SiO_2$) catalyst. However, several side products up to C_6 hydrocarbons were formed. Further research into Pt based catalyst have resulted in bimetallic system such as Co-Pt@NaY [13], Pt-Bi@ZSM-5 [20] and Pt-Sn@ZSM-5 [21]. Bimetallic catalyst are found to be more stable and coke resistant, lesser prone to deactivation. Further, use of zeolite as support has helped in enhancing the selectivity of the product obtained.

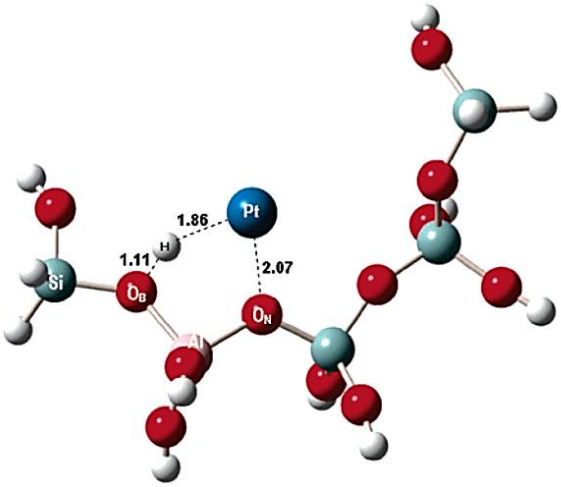

Figure 2: *Platinum anchored within the aluminosilicate framework. Color codes: red- O, dark blue- Pt, light blue- Si, white- H, light red- Al (printed with permission from ref. 22).*

In all these catalysts, Pt is anchored within the alumino-silicate framework. Theoretical studies have shown that Platinum simultaneously interacts with the Brønsted proton and lattice oxygen of the zeolite framework (as shown in Figure 2). The lattice oxygen transfers the electron into the d-orbitals of Pt which increases the overall electron density which destabilizes the system. However, the Brønsted proton present withdraws the excess electron density and stabilizes Pt within the framework [22].

Terrace site (111) of Pt is found to be active for methane activation [21, 23, 24]. The mechanism of methane activation over platinum is still under debate. However, one of the widely accepted mechanism is the agostic interaction [10, 25, 26, 27] between transition metal and methane. In this mechanism, methane donates electron into the metal acceptor orbital which results in C-H bond stretching. M-H-C interaction is further strengthened by backbonding of the metal d-orbitals with the antibonding sigma orbital of methane. This results in cleavage of the C-H bond and oxidative addition to the metal center. During the reaction most of the terrace sites are occupied by CH_2*, CH*, C* intermediates. The C-C coupling takes place on the surface and results in formation of olefins and aromatic molecules.

Studies have shown that Sn acts as a promoter. Isobutane dehydrogenation improved upon addition of Sn to Ni supported on SiO_2 [29]. This was attributed to the formation of Ni_3Sn which increased the electronic repulsion of isobutane on the surface which facilitated the desorption of isobutene and thereby improving the selectivity of the product formed. Addition of Sn modified the electronic property of the catalytic surface and thereby improved the coke resistance and catalytic performance in Pt-Sn/ SAPO (Silico-Alumino Phosphate) [28] zeolite for propane dehydrogenation. Similar effects were observed for NOCM over Pt-Sn/ZSM-5 catalyst [21].

2.2 Scope of present study

There are several reports that show the effect of synthesis strategy on catalyst performance, stability, product selectivity and deactivation. Modifying the synthesis strategy in turn modifies the metal support interaction which affects the catalytic performance. A report on Pt wet impregnation over Sn-modified ZSM-5 showed better stability and low deactivation of the catalyst during propane dehydrogenation [23].

Guo X. *et al* [18] showed that Fe-SiO_2 prepared by ball milling performed better in terms of coke resistance and product selectivity as compared to Fe-SiO_2 prepared by wet impregnation and sol gel method This was attributed to the redistribution of Fe on the silica support resulting in the formation of Si-Fe-C which acted as the active site for non-oxidative coupling of methane.

Another report on Pt supported on MCM-41 and SiO_2 showed that Pt-MCM-41 prepared by sol gel method showed better methane activation compared to Pt -SiO_2. Further, Pt-SiO_2 prepared by sol gel method showed better methane activation compared to that prepared by wet impregnation. Modification of electron density of Pt due by strong metal support interaction giving rise to electron deficient Pt sites which were responsible for the high catalytic activity [12].

Pt based bimetallic systems supported on zeolites have been reported for non-oxidative coupling of methane. Pt-Bi/ZSM-5 prepared by wet impregnation showed 2% methane conversion and 90% selectivity for ethylene at 650 ^oC [20]. Pt-Sn supported on ZSM-5 prepared by wet impregnation showed very low conversion of methane (0.2 %) but with higher selectivity (90%) for ethylene at 700 ^oC [21].

In the present study, efforts have been made to vary the synthesis strategy of Pt-Sn based ZSM-5 system and to understand its effect on the methane conversion and selectivity of the product formed. The catalyst has been prepared by two different methods. Firstly, Sn modified ZSM-5 was synthesised by hydrothermal synthesis which was then impregnated with Pt. In the second method, Pt and Sn was simultaneously added at the time of hydrothermal synthesis. The catalyst prepared has been used to study non-oxidative coupling of methane.

2.3 Experimental Section:

2.3.1 Hydrothermal synthesis of ZSM-5 using sodium silicate solution as the silica source.

In a typical procedure, a 0.1575 g $Al_2(SO_4)_3.16\ H_2O$ was added to 2.5 ml, water containing 0.425 g of H_2SO_4. The mixture was stirred for 10 mins. Tetrapropyl ammonium bromide which acts as a structure directing agent was added to the above solution. The resultant solution was labelled as solution A. Solution B was prepared by

adding 5.46 g of sodium silicate to 312 μL water. Solution A was then added to solution B and stirred for 30 mins. It was left for crystallisation in an autoclave at 180 ^{o}C for 7 days under autogenous pressure.

After 7 days, the product was recovered by centrifugation and was washed using ethanol. The precipitate was collected and dried overnight. The dried sample was calcined at 600 ^{o}C for 4 hours at 5 ^{o}C/min ramp rate to remove the structure directing agent. The product obtained was characterized by PXRD. It was observed that the peak corresponding to unreacted silica appeared in the PXRD pattern. A modified approach method where the silica source, sodium silicate was replaced with tetraethyl orthosilicate.

2.3.2 Hydrothermal synthesis of ZSM-5 using tetraethyl orthosilicate as the silica source [30].

A 0.32 g $Al_2(SO_4)_3.16\ H_2O$ (corresponding to Si/Al =30) was added to 4 ml, 1 M aqueous tetrapropyl ammonium hydroxide solution. The resultant solution was labelled as solution A. Solution B was prepared by dropwise addition of tetraethyl orthosilicate to 3.47 ml of 1 M aqueous tetrapropyl ammonium hydroxide solution under vigorous stirring. Solution A was then added to solution B. the resultant solution was stirred for 10 mins. It was then transferred into an autoclave and kept for crystallisation at 180 ^{o}C for 4 days under autogenous pressure. The weight of the Al and Si precursors mentioned above corresponds to Si/Al ratio of 30. The ZSM-5 corresponding to Si/Al ratio of 50 and 100 was prepared by following the similar procedure.

The product was recovered by centrifugation and was washed using ethanol. The precipitate was collected and dried overnight. The dried sample was calcined at 600 ^{o}C for 4 hours at 5 ^{o}C/min ramp rate to remove the structure directing agent (tetrapropyl ammonium hydroxide. The product obtained after 4 days was analysed by PXRD. The characteristic peaks corresponding to ZSM 5 appeared in the PXRD pattern which confirmed the formation of the zeolite.

2.3.3 Hydrothermal synthesis of Sn-ZSM-5

Sn-ZSM was synthesised by modifying a previously reported procedure [23, 30] wherein a 0.32 g $Al_2(SO_4)_3.16\ H_2O$ (corresponding to Si/Al =30) was added to 4 ml, 1 M aqueous tetrapropyl ammonium hydroxide solution. The resultant solution A was added to

Solution B prepared by dropwise addition of 6 ml of tetraethyl orthosilicate to 3.47 ml of 1 M aqueous tetrapropyl ammonium hydroxide solution under vigorous stirring. To the above solution, 0.66 ml, 0.1 M $SnCl_2.2H_2O$ solution was added. The mixture was stirred vigorously for 15 mins. It was then transferred into an autoclave and kept for crystallisation at 180 ^oC for 4 days under autogenous pressure.

The product recovered by centrifugation was washed with ethanol. The precipitate was collected and dried overnight. The dried sample was calcined at 600 ^oC for 4 hours at 5 ^oC/min ramp rate to remove the structure directing agent (tetrapropyl ammonium hydroxide). The product obtained was labelled Sn-ZSM-5.

2.3.4 Synthesis of Pt@ Sn-ZSM-5 by wet impregnation [23]

1 g of the prepared Sn-ZSM-5 was dispersed in 20 ml ethanol. To this, 0.5 ml of 0.1 M H_2PtCl_6 (equivalent to 1 wt% Pt) was added. The resultant dispersion was sonicated for 10 mins in a bath sonicator. It was then kept under continuous stirring at 80 ^oC to remove the solvent. The obtained sample was then reduced under 10% H_2 atmosphere at 600 ^oC for 4 hours at 5 ^oC/min ramp rate in a tubular furnace.

2.3.5 Hydrothermal synthesis of Pt-Sn@ZSM-5 (I.S.)

Solution A, B prepared by the above procedure was mixed under vigorous stirring. A 0.66 ml, 0.1 M $SnCl_2.2H_2O$ solution was added to it. This was followed by the addition of 0.4 ml, 0.1 H_2PtCl_6 solution under vigorous stirring. It was then transferred into an autoclave and kept for crystallisation at 180 ^oC for 4 days under autogenous pressure.

The product was recovered by centrifugation and was washed using ethanol. The precipitate was collected and dried overnight. The dried sample was calcined at 600 ^oC for 4 hours at 5 ^oC/min ramp rate to remove the structure directing agent (tetrapropyl ammonium hydroxide). The product obtained was reduced under 10% H_2 atmosphere at 600 ^oC for 4 hours at 5 ^oC/min ramp rate in a tubular furnace.

2.3.6 Catalytic Performance for Non-oxidative coupling of methane

The catalyst performance was studied using a fixed bed reactor wherein, 200 mg of the prepared catalyst was loaded into a quartz tube reactor (9 mm inner diameter). The catalyst was pretreated under H_2 atmosphere (10 sccm) at 600 ^oC for an hour. The reactor

was then purged with N_2 and the temperature was raised to 850 ^oC. The reactor was then purged with a gas mixture of methane (10 sccm) and nitrogen (20 sccm). The temperature was further raised to 875 ^oC and the readings were taken at 1 hour interval over a period of 12 hour time on stream.

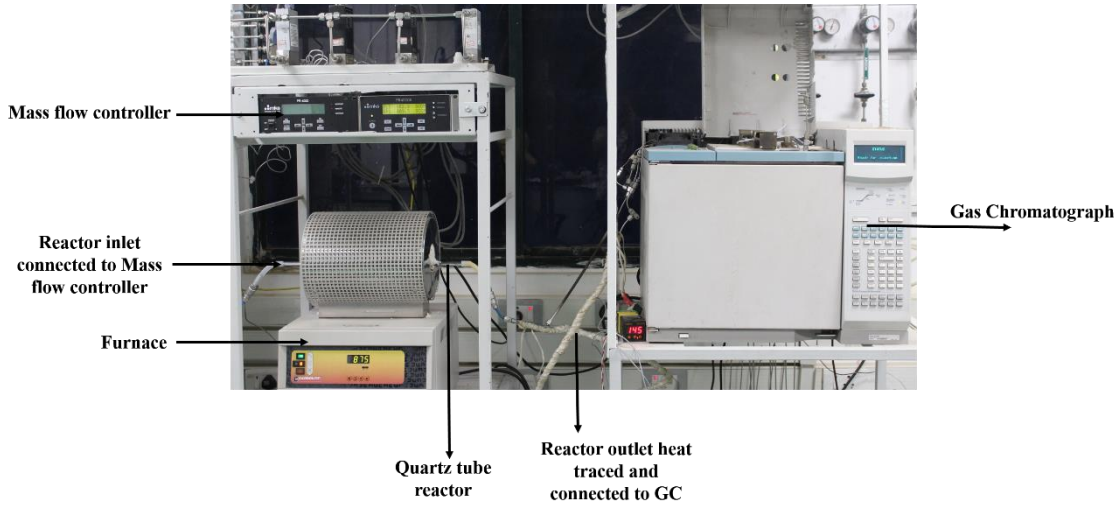

Figure 3: *The reaction set up to study the catalytic activity.*

2.4 Sample Characterizations:

Powder X-Ray Diffraction measurements were recorded using Rigaku using Cu Kα radiations. The morphologies of the sample was examined using Field Emission scanning electron microscopy ZEISS Gemini 500 FESEM and FESEM FEI Nova-Nano SEM-600. The elemental composition was determined by Energy Dispersive X-Ray Scattering technique using Tecnai, T20. The transmission electron microscopy images were obtained using JEOL JEM-3010 at 300 kV and Tecnai, T20 at 200 kV. The products obtained were separated and analysed using gas chromatograph, GC 6890N equipped with FID detector and alumina bond column. Temperature programmed oxidation and temperature programmed desorption studies were done using BELCAT II instrument. Nitrogen adsorption-desorption isotherms were obtained using Quantachrome Autosorb iQ.

2.5 Results and Discussion

2.5.1 Characterizations

As part of the present study, the synthesis of zeolite ZSM-5 was optimised. The synthesized zeolites were characterised by PXRD. Figure 4 shows the PXRD pattern of the synthesized zeolites. Figure 4a shows a broad peak of amorphous silica [31] at 2θ = 24.9 degrees indicating that the silica source used i.e. sodium silicate is not resulting in the formation of ZSM-5 even after 7 days of autoclavation. PXRD patterns in figure 4b show characteristic peaks 2θ = 8.01, 8.88, 23.14, 23.96 and 24.46 degrees corresponding to (101), (200), (051), (033) and (313) planes respectively indicate the formation of the ZSM-5 upon using tetraethyl ortho silicate (TEOS) as the silica source within 4 days of autoclavation. The above synthesised zeolite has Si/Al ratio= 30. Further, zeolites with different Si/Al ratio corresponding to 50 and 100 were also synthesised.

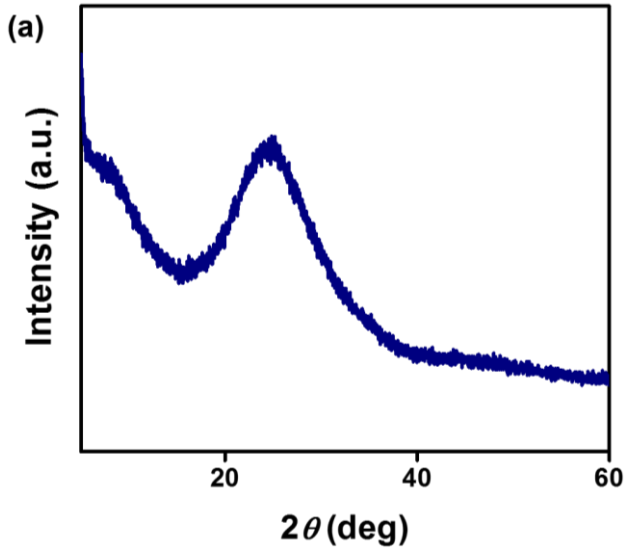

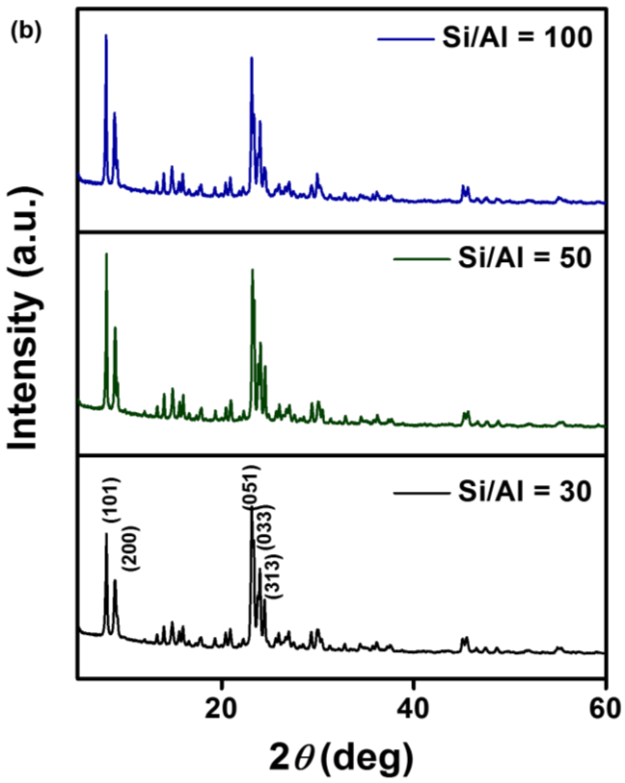

Figure 4: *Powder X-ray diffraction pattern of* **(a)** *amorphous silica obtained upon using sodium silicate solution as the silica source,* **(b)** *ZSM-5 with Si/Al= 30, 50, 100*

In the present study, the catalyst were prepared by two different methods. Firstly, Sn modified ZSM-5 (with Si/Al = 30) was synthesised by hydrothermal synthesis which was then impregnated with Pt (henceforth Pt@Sn-ZSM-5). In the second method, Pt and Sn were simultaneously added at the time of hydrothermal synthesis (henceforth Pt-Sn@ZSM-5 (I.S.)). The catalyst thus prepared were characterized by powder X- Ray Diffraction (figure 5). Here, the characteristic peaks of ZSM-5 at 2θ = 8.01, 8.88, 23.14, 23.96 and 24.46 degrees peaks corresponding to (101), (200), (051), (033) and (313) planes respectively was observed. This indicates that the metal loading has not resulted in any deformation of the aluminosilicate framework. Furthermore, low intensity peaks at $2\theta = 40^{o}$ corresponding to (111) plane characteristic of presence of Pt was observed in the PXRD pattern. However the peak corresponding to Sn at $2\theta = 30^{o}$ is not distinctly visible. Absence of peaks with significant intensity corresponding to Pt and Sn may be attributed to the low loading of Pt and Sn. Hence, to further confirm the presence of Pt and Sn, EDS analysis was performed.

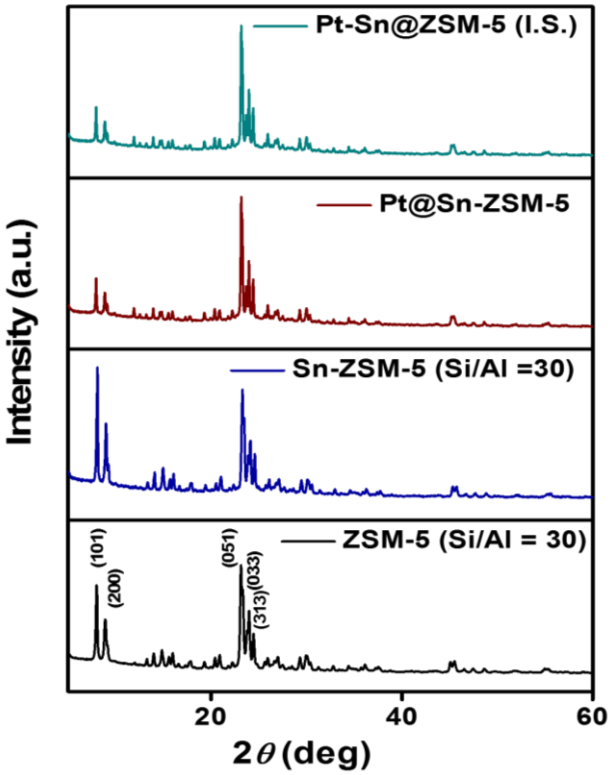

Figure 5: *Powder X-ray diffraction pattern of synthesized catalysts.*

The EDS data (figure 6d) shows the presence of 0.78 weight percent of Sn and 0.25 weight percent of Pt in Pt@Sn-ZSM-5 catalyst. Transmission electron microscopy (TEM) images of Pt@Sn-ZSM-5 shows square shaped particles. The size of the metal particles loaded on to the zeolite were found to be in 1.7 to 2 nm range.

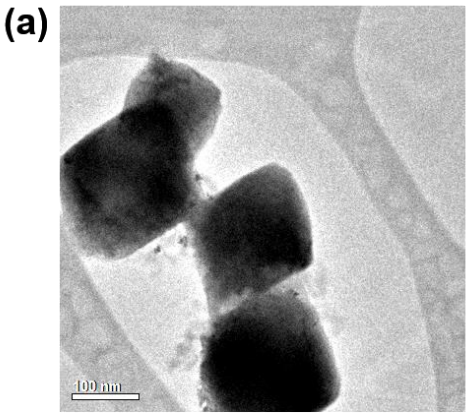

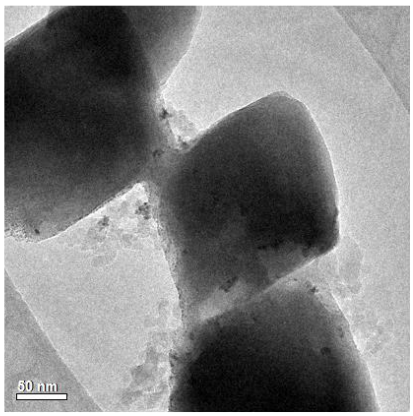

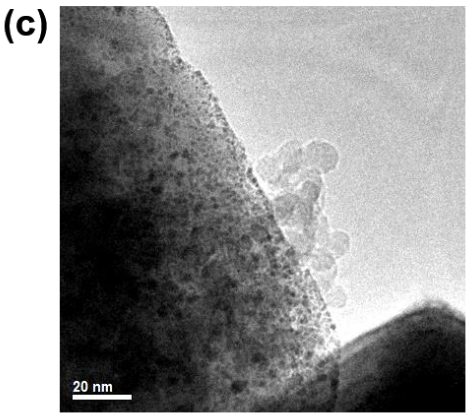

(d)

Element	Weight %
O(K)	34.35
Al(K)	0.33
Si(K)	64.26
Sn(K)	0.78
Pt(L)	0.25

Figure 6: *Transmission electron microscopy (TEM) images of Pt@Sn-ZSM-5 under* **(a)**, **(b)** *low magnification,* **(c)** *high magnification and* **(d)** *Energy dispersive x-ray scattering (EDS) analysis showing presence of Pt and Sn in the zeolite framework.*

The surface area of the prepared catalysts were determined from N_2 adsorption-desorption isotherm (figure 7). The absence of hysteresis in the isotherms indicates the microporosity of the prepared catalyst. The surface area of the prepared catalysts were calculated by Bruner- Emmet- Teller method and was found to be 317 m^2/g for Pt-Sn @ZSM-5 and 362 m^2/g for Pt@Sn-ZSM-5.

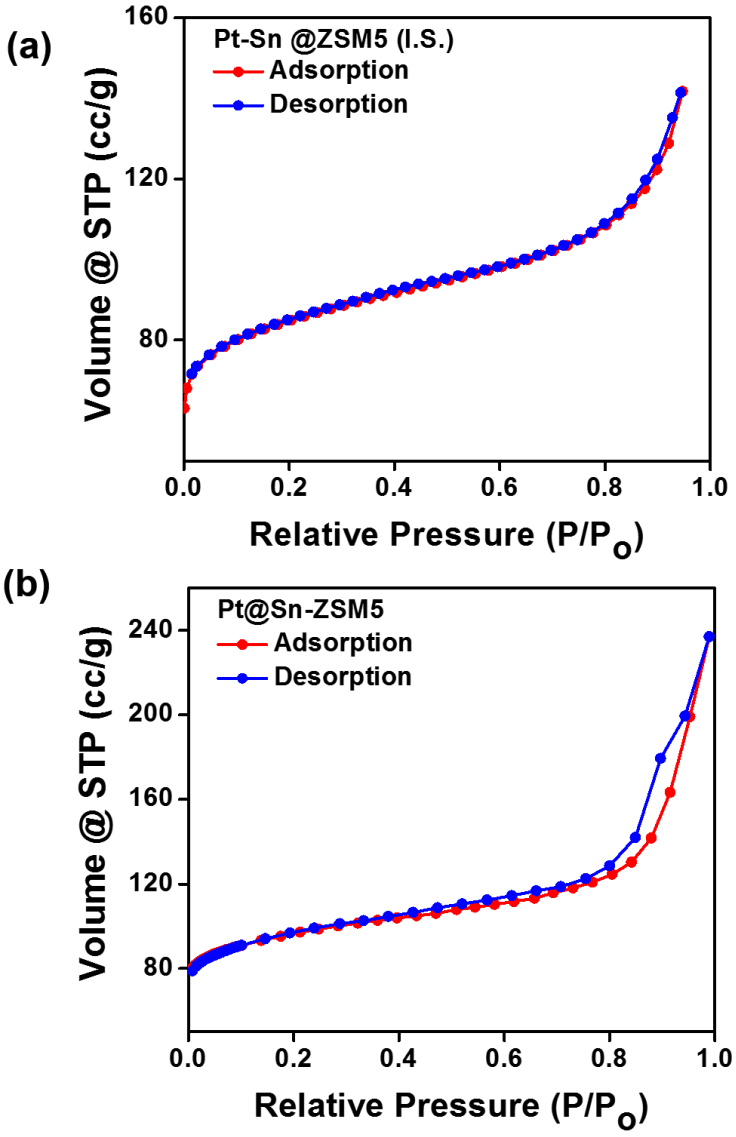

Figure 7: *N_2 adsorption-desorption isotherm of* **(a)** *Pt-Sn@ZSM-5 prepared by hydrothermal synthesis (HS),* **(b)** *Pt@Sn-ZSM-5.*

Fourier transform infrared spectroscopy (FTIR) spectra of the prepared catalyst (figure 8) gives a qualitative picture of the incorporation of the metal ions into the aluminosilicate framework. Figure 7a shows the spectra of ZSM-5 (with Si/Al =30). A broad peak at 3420 cm^{-1} is characteristic of the hydroxyl group present in the aluminosilicate framework [32, 33]. The peak corresponding to asymmetric stretching of Si-O-Si and Si-O-Al appears in the 900 to 1200 cm^{-1} region [32, 33]. Incorporation of metal (here Pt and Sn) into the framework results in the broadening of this peak [23].

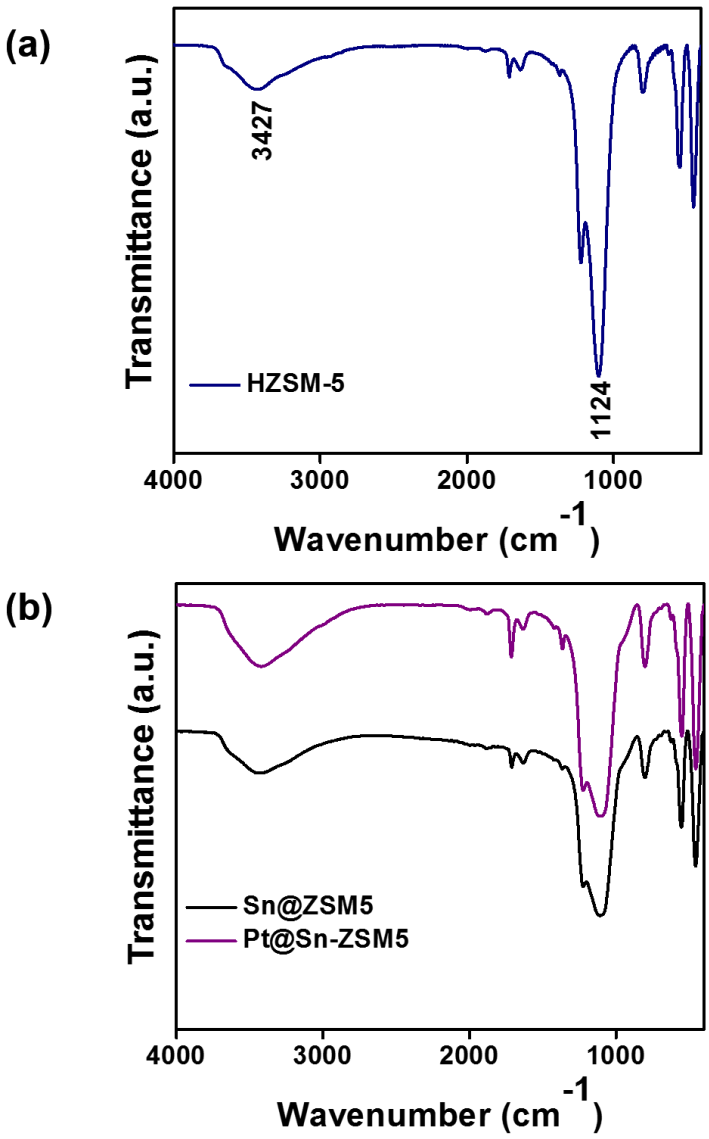

Figure 8: *Fourier transform Infrared spectra (FTIR) of* **(a)** *ZSM-5* **(b)** *Sn-ZSM-5 and Pt@Sn-ZSM-5.*

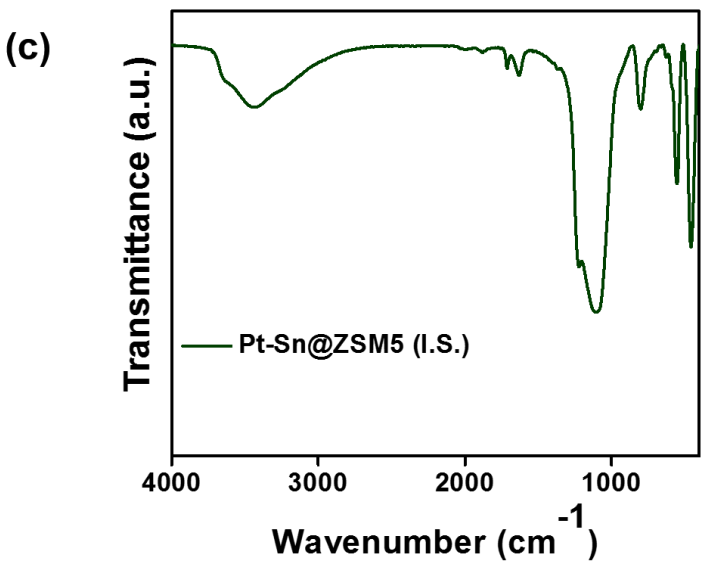

Figure 8: (c) *Fourier transform Infrared spectra (FTIR) of Pt-Sn@ZSM-5 (I.S.).*

The acid sites present in the zeolite may be probed using temperature programmed desorption (TPD). During TPD, adsorption and desorption of a probe molecule (herein, ammonia (NH_3)) is used to determine the acidity of the catalyst. The results (shown in Figure 9) of TPD studies show that the total acid site density of Pt@Sn-ZSM-5 is more compared to Pt-Sn@ZSM-5. The ammonia TPD profile for both the catalyst show a low temperature peak (174.6 ^oC) which correspond to sites with low acidity (Lewis acid sites) and the peak at high temperature (470 ^oC and above) correspond to sites with high acidic strength (Brønsted acid sites) [34, 35, 36].

No.	Start time (sec)	End time (sec)	Time width (sec)	Peak position (sec)	Peak position (?C)	Area (count)	mmol	mmol/g	log(W/F)+3
1	1910	2907	998	2296	174.6	172,959	0.008	0.128	-3.678
2	2908	4524	1617	3986	469.2	68,638	0.003	0.051	-4.183
3	4525	5546	1022	5155	662.5	104,223	0.005	0.077	-4.415

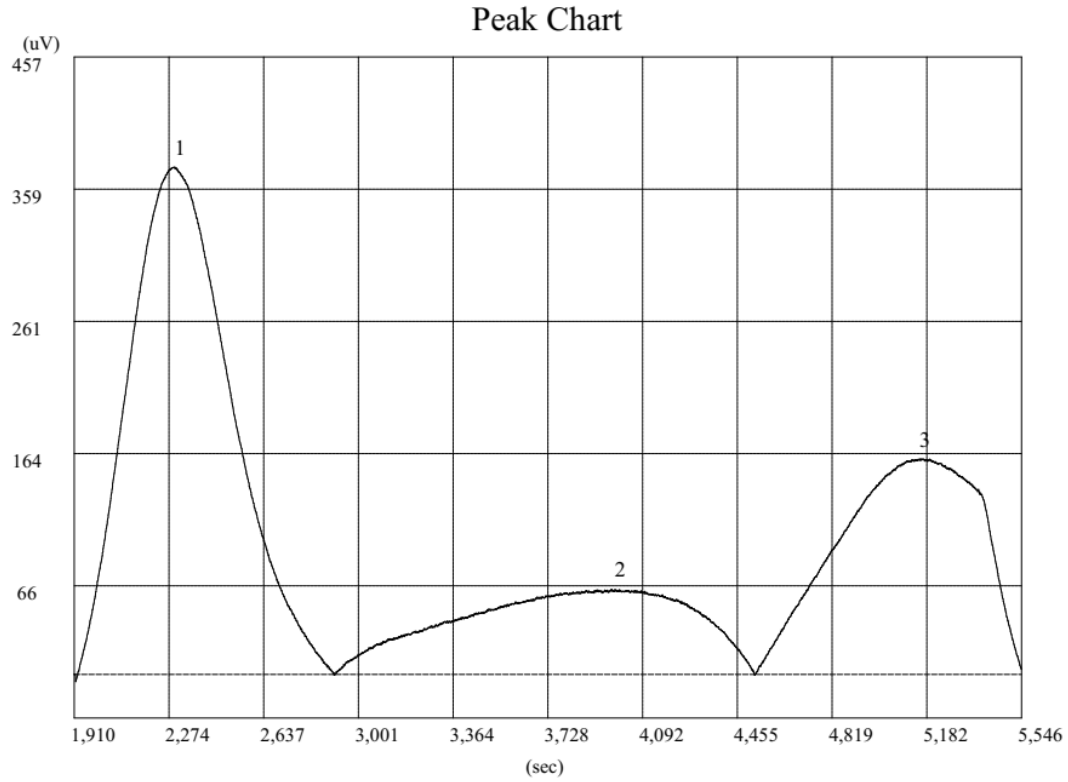

Figure 9: (a) NH_3-TPD profile of Pt@Sn-ZSM-5.

No.	Start time (sec)	End time (sec)	Time width (sec)	Peak position (sec)	Peak position (?C)	Area (count)	mmol	mmol/g	log(W/F)+3
1	1838	2761	924	2279	171.8	154,850	0.007	0.110	-3.633
2	2762	4900	2139	4022	475.3	101,602	0.005	0.072	-4.153

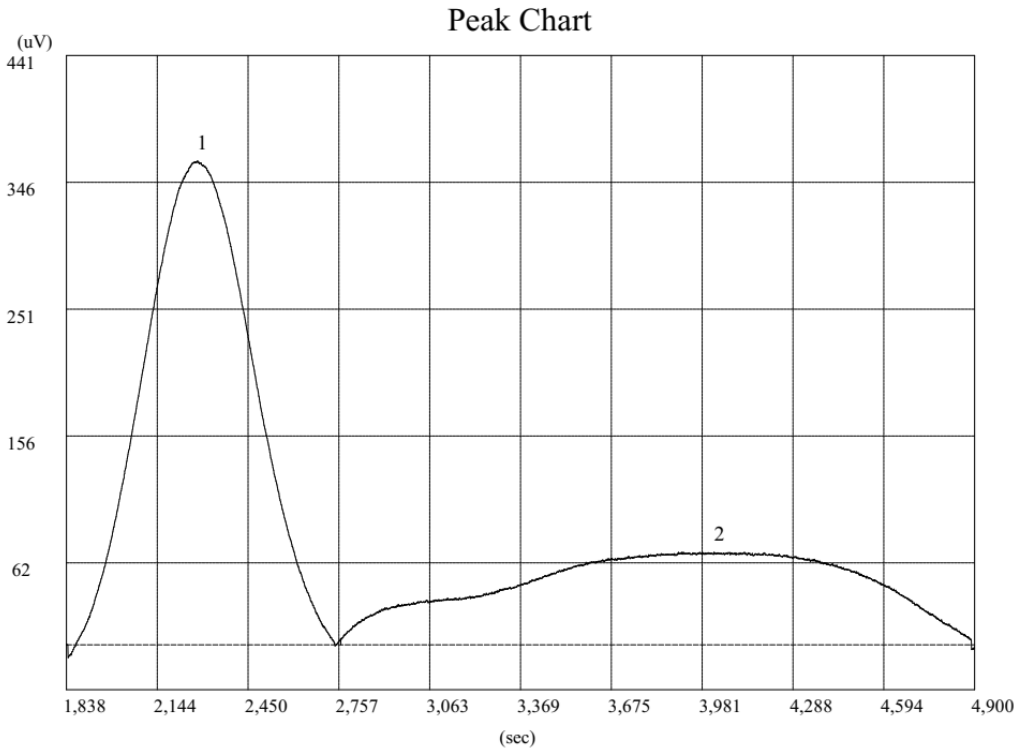

Figure 9: (b) NH_3-TPD profile of Pt-Sn@ZSM-5 (I.S.).

2.5.2 Catalytic Activity

The catalytic activity was calculated by the following formulae

$$\% \text{ Methane Conversion} = \frac{\boldsymbol{moles\ of\ methane\ (in) - moles\ of\ methane\ (out)}}{\boldsymbol{moles\ of\ methane\ (in)}} \times \mathbf{100}\ \%$$

$$\% \text{ Selectivity } (S_i) = \frac{\boldsymbol{moles\ of\ product\ i\ formed}}{\boldsymbol{total\ moles\ of\ product\ formed}} \times \mathbf{100}\ \%$$

Where, in and out correspond to molar flow of methane at inlet and outlet.

The temperature dependent study (Figure 10) of non-oxidative coupling of methane (NOCM) over Pt-Sn@ZSM-5 (fig 10a) and Pt@Sn-ZSM-5 (fig 10b) shows that NOCM begins at 875^{o}C. Prior to 875 ^{o}C, conversion of methane is observed but no gaseous products are observed at the outlet. The initial rise in conversion may be attributed to the induction period during which the catalyst gets saturated with methane. Methane gets

chemisorbed on the catalyst site and undergoes oligomerisation to form polymeric species. At 875 ^{o}C, dehydrogenation takes place and the product formed desorbs from the surface. As a result, an increase in product selectivity is observed. There is further increase in methane conversion accompanied by product formation. At 875 ^{o}C, Pt-Sn@ZSM-5 shows ~85% total olefin (C_2+C_3) selectivity at 4% methane conversion whereas the catalyst Pt@Sn-ZSM-5 (fig. 10b) shows comparatively low methane conversion of ~0.5 % with similar total olefin selectivity around 88%.

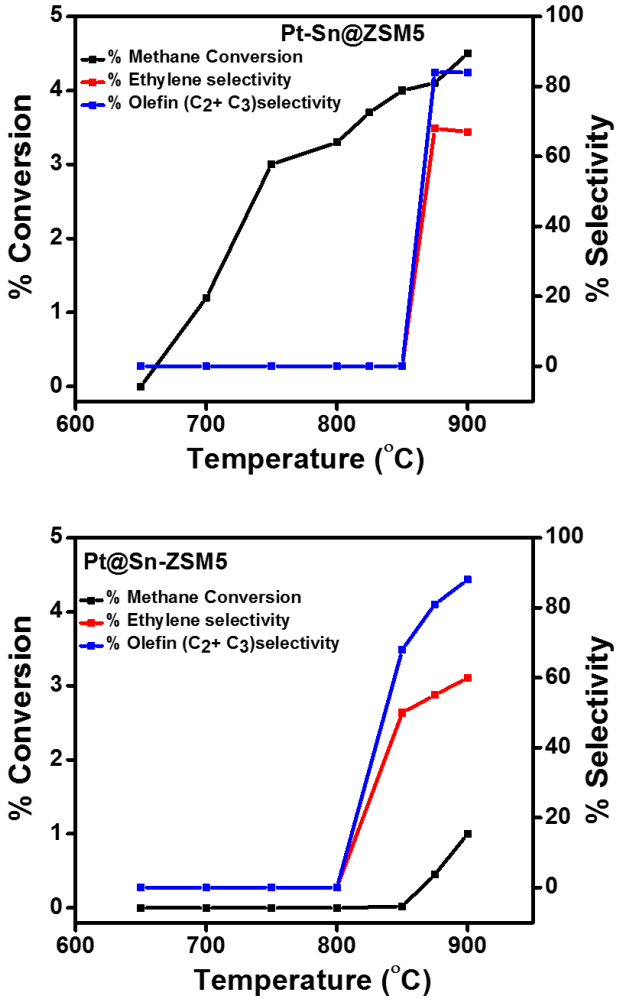

Figure 10: *Temperature dependent study of NOCM over* **(a)** *Pt-Sn@ZSM-5 (I.S.)* **(b)** *Pt@Sn-ZSM-5. Reaction conditions: CH_4 flow = 10 sccm, N_2 flow = 20 sccm, catalyst weight = 200 mg.*

The time dependent study (Figure 11) upto 12 hours show that in case of Pt-Sn@ZSM-5, the catalyst was stable upto 6 hours and the conversion increased continuously during this time period and attained a maximum conversion of 7 %. After 6 hour, the

deactivation of the catalyst is observed due to coke formation which results in decreased conversion. However, the total olefin selectivity remained constant at ~ 90%. On the other hand, Pt@Sn-ZSM-5 showed continuous increase in methane conversion. The maximum conversion obtained was ~7 % as observed in the former case. However, the catalyst does not show any deactivation during the time of study. This observed increase in activity can be attributed to the presence of some bare Pt atoms on the support surface. Since Pt is known to be more active than bimetallic Pt-Sn system hence this justifies the increased activity which again is proved by higher amount of coke deposited as shown in figure 12c.

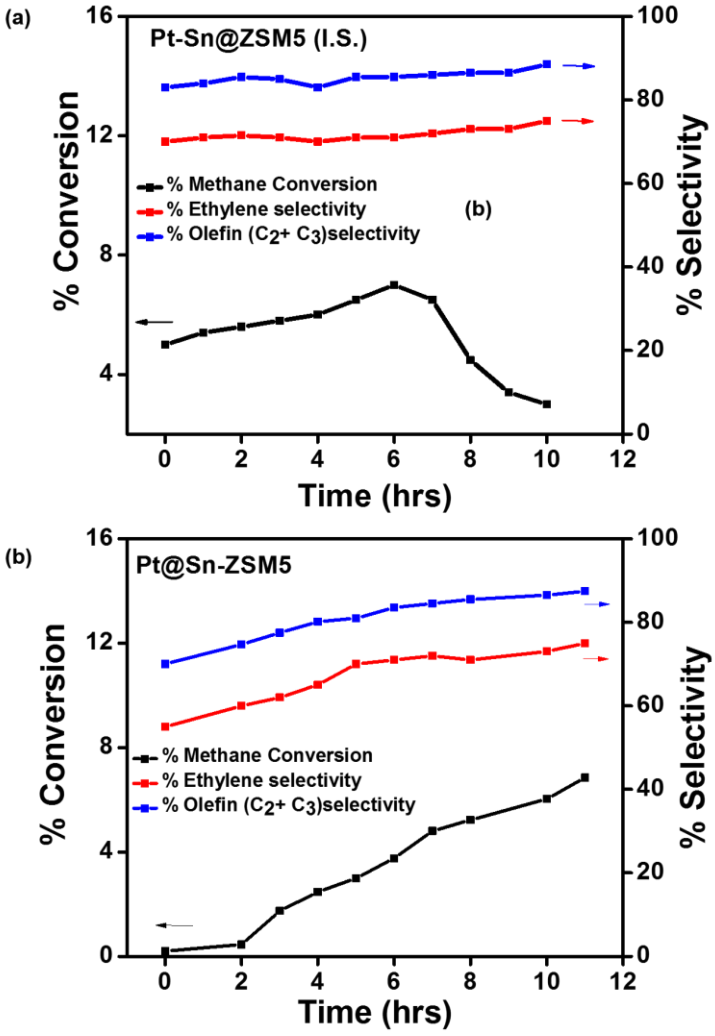

Figure 11: *Time dependent study of non-oxidative coupling of methane (NOCM) over* **(a)** *Pt-Sn@ZSM-5 (I.S.) and* **(b)** *Pt@Sn-ZSM-5. CH_4 flow = 10 ml/min and N_2 flow = 20 ml/min, amount of catalyst taken = 200 mg, temperature = 875 ^oC.*

The coke deposited during the reaction was probed by thermogravimetric analysis (TGA) and by temperature programmed oxidation (TPO). The TGA data (shown in Figure 12) of the catalyst before NOCM show that the catalyst is stable upto 1000 ^{o}C. However, a slight weight loss is observed below 500 ^{o}C which can be attributed to the loss of strongly adsorbed water molecules present in the zeolitic framework. TGA of the catalyst post NOCM, showed loss in weight owing to the presence of the coke deposited during the reaction. Figure 12c compares the results of TGA and TPO of the coke deposited on the catalyst. The amount of coke deposited determined by TGA was found to be comparable to the values obtained from TPO studies.

The results show that more amount of coke is deposited on Pt@Sn-ZSM-5 as compared to Pt-Sn@ZSM-5. This may be attributed to the high acid site density on Pt@Sn-ZSM-5 as a result of which more amount of methane is strongly adsorbed over the catalyst surface and is getting converted to coke.

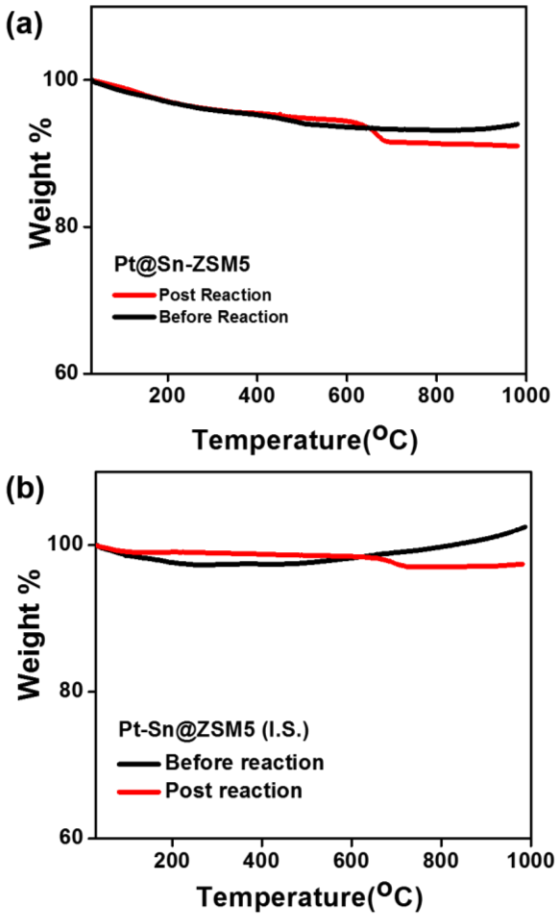

(c)

Catalyst	Coke Deposited (g/g_{cat})	
	TPO	**TGA**
Pt-Sn@ZSM5	**0.01**	**0.02**
Pt@Sn-ZSM5	**0.15**	**0.06**

Figure 12: *Thermogravimetric analysis (TGA) of* **(a)** *Pt-Sn@ZSM-5,* **(b)** *Pt@Sn-ZSM-5 prepared by hydrothermal synthesis (I.S.)* **(c)** *Estimation of coke deposited on the catalyst by TPO and TGA.*

2.6 Conclusion

In the present study, Pt-Sn supported on zeolite, ZSM-5 have been employed for non-oxidative coupling

of methane (NOCM). The catalysts were prepared by hydrothermal synthesis. The metal particles loaded on to the zeolites were found to be 1.7-2 nm in size.

The NOCM showed an initial induction period in case of Pt-Sn@ZSM-5 (I.S.) during which significant conversion was observed although no gaseous products were formed. This may be attributed to the chemisorption of methane onto the active sites. Once the catalyst surface is saturated, the adsorbed methane undergo oligomerisation to form polymeric species. However, the time on stream study shows that Pt-Sn@ZSM-5 deactivates within 10 hours owing to the coke formation. On the other hand, Pt@SnZSM-5 remained active during the time of study. The maximum conversion and total olefin selectivity was found to be comparable in both cases which shows that Pt is the active component while Sn helps in making the surface coke resistant.

The results obtained in this study are very promising compared to the previously reported work using Pt-Sn@ZSM-5 and Pt-Bi@ ZSM-5 catalyst. It is further interesting to note that propylene formation was observed in our study which is not the case in the previous reports. The following table compares the present results with the reported ones.

Catalyst	Metal Loading (wt%)	Synthesis strategy	Conversion (%)	Selectivity (%)
Pt-Bi@ZSM-5[20]	Pt-1% Bi-0.8 %	Wet impregnation	4 %	90 % (C_2)
Pt-Sn@ZSM-5[21]	Pt-1% Sn-2 %	Wet impregnation	0.2%	90% (C_2)
Pt@Sn-ZSM-5 (this work)	Pt-1% Sn-1 %	Hydrothermal synthesis	6.85 %	87% (C_2+C_3 olefin)
Pt-Sn@ZSM-5 (I.S.) (this work)	Pt-1% Sn-1 %	Hydrothermal synthesis	7%	89% (C_2+C_3 olefin)

2.7 Future Directions

As Pt is a noble metal, efforts will be put in to decrease the Pt loading on the catalyst. Further, time on stream study for longer durations have to be performed to comment on the catalyst deactivation and stability. XPS analysis to determine the nature of the active sites would be performed. ZSM-5 with varying acid site density will be employed to study the effect of acidity on catalytic activity. Further, control studies would be done to compare the catalytic activity.

2.8 References

1. Tang, P.; Zhu, Q.; Wu, Z.; Ma, D. Methane Activation: The Past and Future. *Energy Environ. Sci.* **2014**, *7* (8), 2580–2591.
2. Arora, S.; Prasad, R. An Overview on Dry Reforming of Methane: Strategies to Reduce Carbonaceous Deactivation of Catalysts. *RSC Adv.* **2016**, *6* (110), 108668–108688.

3. Kinetics of methane steam reforming on a Ni on alumina-titania catalyst A.E. Castro Luna and A.M. Becerra. *Science (80).* **1997**, *61* (2), 369–374.
4. Liu, C. J.; Ye, J.; Jiang, J.; Pan, Y. Progresses in the Preparation of Coke Resistant Ni-Based Catalyst for Steam and CO_2 Reforming of Methane. *ChemCatChem* **2011**, *3* (3), 529–541.
5. Pierre S.; Xiulian P., J.; Xinhe B. Direct conversion of methane to value added chemicals over heterogenous catalysts: challenges and prospects. *Chem. Rev.* **2017**,117, 8497-8520.
6. Li, C.; Yan, W.; Xin, Q. Interaction of Methane with Surface of Alumina Studied by FT-IR Spectroscopy. *Catal. Letters* **1994**, *24* (3–4), 249–256.
7. Knoezinger, H.; Huber, S., IR Spectroscopy of Small and Weakly Interacting Molecular Probes for Acidic and Basic Zeolites. *ChemInform* **2010**, *29* (41).
8. Agarwal, V.; Metiu, H. Hydrogen Abstraction Energies and Ammonia Binding to BEA, ZSM-5, and α-Quartz Doped with Al, Sc, B, or Ga. *J. Phys. Chem. C* **2015**, *119* (28), 16106–16114.
9. Chen, L.; Lin, L.; Xu, Z.; Zhang, T.; Liang, D.; Xin, Q.; Ying, P. Interaction of Methane with Surfaces of Silica, Aluminas and HZSM-5 Zeolite. A Comparative FT-IR Study. *Catal. Letters* **1995**, *35* (3–4), 245–258.
10. Zheng, X.; Blowers, P. A Computational Study of Methane Catalytic Reactions on Zeolites. *J. Mol. Catal. A Chem.* **2006**, *246* (1–2), 1–10.
11. Guczi, L.; Sarma, K. V.; Borkó, L. Non-Oxidative Methane Coupling over Co-Pt/NaY Bimetallic Catalysts. *Catal. Letters* **1996**, *39* (1–2), 43–47.
12. Eswaramoorthy, M.; Niwa, S.; Toba, M.; Shimada, H.; Raj, A.; Mizukami, F. The Conversion of Methane with Silica-Supported Platinum Catalysts : The Effect of Catalyst Preparation Method and Platinum Particle Size. *Catal. Letters,***2001**, *71* (1), 55–61.
13. Fu, G.; Xu, X.; Lu, X.; Wan, H. Mechanisms of Methane Activation and Transformation on Molybdenum Oxide Based Catalysts. *J. Am. Chem. Soc.* **2005**, *127* (11), 3989–3996.
14. Tshabalala, T. E.; Coville, N. J.; Scurrell, M. S. Applied Catalysis A : General Dehydroaromatization of Methane over Doped Pt / Mo / H-ZSM-5 Zeolite

Catalysts : The Promotional Effect of Tin. *"Applied Catal. A, Gen.* **2014**, *485*, 238–244.

15. Ding, W.; Li, S.; Meitzner, G. D.; Iglesia, E. Methane Conversion to Aromatics on Mo/H-ZSM-5: Structure of Molybdenum Species in Working Catalysts. *J. Phys. Chem. B* **2001**, *105* (2), 506–513.
16. Szécsényi, Á.; Li, G.; Gascon, J.; Pidko, E. A. Mechanistic Complexity of Methane Oxidation with H2O2by Single-Site Fe/ZSM-5 Catalyst. *ACS Catal.* **2018**, *8* (9), 7961–7972.
17. Ohnishi, R.; Liu, S.; Dong, Q.; Wang, L.; Ichikawa, M. Catalytic Dehydrocondensation of Methane with CO and CO_2 toward Benzene and Naphthalene on Mo/HZSM-5 and Fe/Co-Modified Mo/HZSM-5. *J. Catal.* **1999**, *182* (1), 92–103.
18. Guo, X.; Fang, G.; Li, G.; Ma, H.; Fan, H.; Yu, L.; Ma, C.; Wu, X.; Deng, D.; Wei, M.; et al. Direct, Nonoxidative Conversion of Methane to Ethylene, Aromatics, and Hydrogen. *Science (80).* **2014**, *344* (6184), 616–619.
19. Sheng, H.; Schreiner, E. P.; Zheng, W.; Lobo, R. F. Non-Oxidative Coupling of Methane to Ethylene Using Mo_2C/[B]ZSM-5. *ChemPhysChem* **2018**, *19* (4), 504–511.
20. Xiao, Y.; Varma, A. Highly Selective Nonoxidative Coupling of Methane over Pt-Bi Bimetallic Catalysts. *ACS Catal.* **2018**, *8* (4), 2735–2740.
21. Huber, G. W.; Gerceker, D.; Miller, J. B.; Rivera-Dones, K. R.; Motagamwala, A. H.; Dumesic, J. A.; Mavrikakis, M. Methane Conversion to Ethylene and Aromatics on PtSn Catalysts. *ACS Catal.* **2017**, *7* (3), 2088–2100.
22. Treesukol, P.; Srisuk, K.; Limtrakul, J.; Truong, T. N. Nature of the Metal-Support Interaction in Bifunctional Catalytic Pt/H-ZSM-5 Zeolite. *J. Phys. Chem. B* **2005**, *109* (24), 11940–11945.
23. Zhang, Y.; Zhou, Y.; Huang, L.; Xue, M.; Zhang, S. Sn-Modified ZSM-5 As Support for Platinum Catalyst in Propane Dehydrogenation. *Ind. Eng. Chem. Res.* **2011**, *50* (13), 7896–7902.

24. Zhang, Y.; Zhou, Y.; Qiu, A.; Wang, Y.; Xu, Y.; Wu, P. Propane Dehydrogenation on PtSn/ZSM-5 Catalyst: Effect of Tin as a Promoter. *Catal. Commun.* **2006**, *7* (11), 860–866.

25. Crabtree, R. H. Alkane C – H Activation and Functionalization with Homogeneous Transition Metal Catalysts : A Century of Progress — a New. *J. Chem. Soc., Dalt. Trans* **2001**, No. 4, 2437–2450.

26. Brookhart, M.; Green, M. L. H.; Parkin, G. Agostic Interactions in Transition Metal Compounds. *PNAS* **2007**, *104* (17), 6908–6914.

27. Crabtree, R. H. Transition Metal Complexation of Sigma Bond. *Angew. Chemie Int. Ed.* **1993**, *32*, 789–805.

28. Nawaz, Z.; Tang, X.; Wang, Y.; Wei, F. Parametric Characterization and Influence of Tin on the Performance of Pt - Sn / SAPO-34 Catalyst for Selective Propane Dehydrogenation to Propylene. *ACS Ind. Eng. Chem. Res.* **2010**, 1274–1280.

29. Zhu, Q.; Wang, G.; Liu, J.; Su, L.; Li, C. E Ff Ect of Sn on Isobutane Dehydrogenation Performance of Ni / SiO_2 Catalyst : Adsorption Modes and Adsorption Energies of Isobutane and Isobutene. *ACS Appl. Mater. Interfaces* **2017**, *9*, 30711–30721.

30. Dong, X.; Shaikh, S.; Vittenet, J. R.; Wang, J.; Liu, Z.; Bhatte, K. D.; Ali, O.; Xu, W.; Osorio, I.; Saih, Y.; et al. Fine Tuning the Diffusion Length in Hierarchical ZSM-5 To Maximize the Yield of Propylene in Catalytic Cracking of Hydrocarbons. *ACS Sustain. Chem. Eng.* **2018**, *6*, 15832–15840.

31. Ren, N.; Subotić, B.; Bronić, J.; Tang, Y.; Dutour Sikirić, M.; Mišić, T.; Svetličić, V.; Bosnar, S.; Antonić Jelić, T. Unusual Pathway of Crystallization of Zeolite ZSM-5 in a Heterogeneous System: Phenomenology and Starting Considerations. *Chem. Mater.* **2012**, *24* (10), 1726–1737.

32. Zhang, S.; Liu, X.; Zhang, Y.; Lv, T.; Zheng, J.; Gao, W. Study on the Synthesis of MFI and FER in the Presence of N-Butylamine and the Property of n-Butylamine in a Confined Region of Zeolites. *RSC Adv.* **2016**, *6*, 114808–114817.

33. Wang, Y.; Wang, R.; Xu, D.; Sun, C.; Ni, L.; Fu, W.; Zeng, S.; Jiang, S.; Zhang, Z.; Qiu, S. Synthesis and Properties of MFI Zeolites with Microporous,

Mesoporous and Macroporous Hierarchical Structures by a Gel-Casting Technique. *New J. Chem.* **2016**, *40*, 4398–4405.

34. Kubic, D.; Kumar, N.; Vena, T.; Heidi, O. Metal - Support Interactions in Zeolite-Supported Noble Metals : Influence of Metal Crystallites on the Support Acidity. *J. Phys. Chem. B*, **2006**, 4937–4946.

35. Wu, W.; Weitz, E. Applied Surface Science Modification of Acid Sites in ZSM-5 by Ion-Exchange : An in-Situ FTIR Study. *Appl. Surf. Sci.* **2014**, *316*, 405–415.

36. Ferenc Lonyi, J. V. On the Interpretation of the NH_3-TPD Patterns of H-ZSM-5 and H-Mordenite. *Microporous Mesoporous Mater.* **2001**, *47*, 293–301.

Chapter -3

Electrochemical CO_2 reduction

3.1 Introduction

Current research scenario is focused on the development of sustainable technology which is energy efficient and environment-friendly. This would help overcome the energy crisis and the global warming problem that the world faces today.

CO_2 is one of the major greenhouse gases that contributes to global warming. A large amount of CO_2 is produced during various combustion processes (Figure 1a). As per the Intergovernmental Panel on Climate Change (IPCC), global emission of CO_2 has reached 35.5 billion tons by 2017(Figure 1b) which has severely harmed the environment. The panel has further recommended that the CO_2 emission must be reduced to 17.9 billion tonnes by 2030 to prevent further damage to the environment. Hence, there is a need to develop methods which would help in mitigating the CO_2 emission.

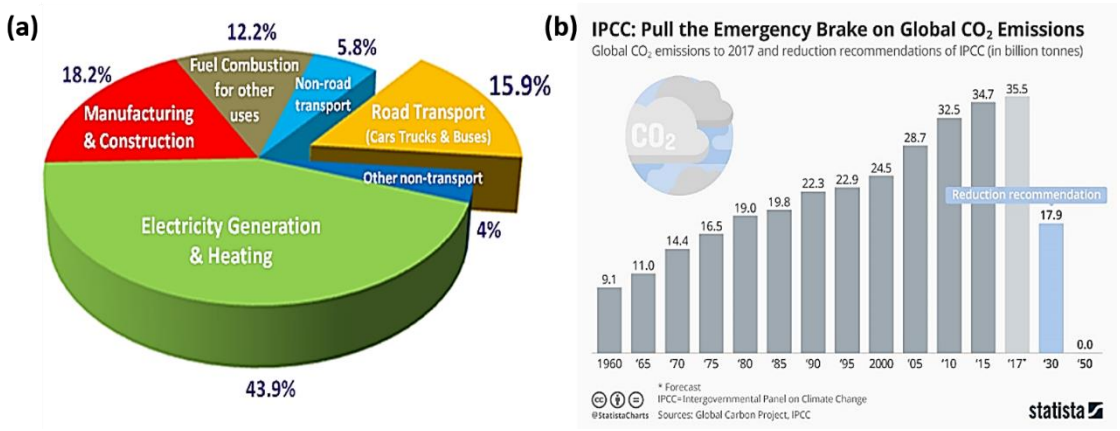

Figure 1: (a) *Sources of Carbon dioxide emission,* **(b)** *Global Carbon dioxide emission (taken from ref.1, ref. 2)*

One of the possible solution would be to use it as a feedstock to produce other value-added chemicals such as HCOOH, CH_3OH, CO etc. Several methods have been employed for the conversion of CO_2 which includes thermocatalysis, photocatalysis, enzymatic conversion, dry reformation etc. However these methods have several drawbacks such as low selectivity for the desired products, requirement of high temperature and pressure, deactivation of the catalyst etc. Reducing CO_2 electrocatalytically is receiving greater attention because of the following reasons [3]: (1) electrochemical reduction takes place under ambient reaction conditions, (2) the product formed can be tuned in terms of selectivity and quantity by varying the potential and

electrolyte, (3) energy requirement for an electrochemical process is low as compared to the conventional processes. Progress in alternative sources of electricity mainly solar has renewed hopes for commercialization of this unconventional approach.

Research into electrochemical CO_2 reduction focusses on three main components: electrochemical cell, electrolyte system and electrocatalysts. Out of these, synthesizing a high performing electrocatalyst is of particular interest because it governs the efficiency with which the reacting molecules interact with the catalyst surface to form the desired product with high selectivity. Essential parameters that determines the choice of the electrocatalyst are; strength of adsorption of the reactant molecules, high faradaic efficiency (measure of efficient charge transfer in a system that facilitates an electrochemical reaction) for the desired product, faster charge transfer and low overpotential.

Carbon dioxide can be converted to several small molecules such as HCOOH, CH_3OH, CO, CH_4 etc. by employing an appropriate electrocatalyst. Several transition metal based electrocatalysts have been developed for CO_2 electroreduction which include metal coordination complexes, metal-organic complexes, metal nanoparticles, metal alloys, oxides, chalcogenides etc. These can be categorized into five main groups based on the products formed as shown in Table 1.

Table1: *Electrocatalyst for CO_2 reduction (adapted from Ref 3.)*

S.No.	Products	Catalyst
1.	HCOOH	Cu, Sn, Pd, Co_3O_4, Pb, Ag, N-doped graphene
2.	CO	Au, Ag, Pd, Zn, Cu
3.	HCHO	B-doped diamonds, Cu NPs/ B-doped diamonds
4.	CH_4, C_2H_4	Cu, Pd, Au
5.	Alcohols (C_xH_xO)	Cu

Reduction of CO_2 to CO is an essential process for the production of syngas (CO + H_2) electrochemically. The electrochemical reduction of CO_2 to CO can be coupled with electrochemical hydrogen evolution reaction to produce syngas which could then be converted to value-added chemicals by Fischer Tropsch synthesis which could make the process economically viable and environment-friendly [5, 6].

CO_2 electroreduction to CO was first reported by Yoshio Hori *et al*. in 1994 [6] wherein they have shown that the reaction proceeds through the formation of COO^- intermediate. Further studies into the reaction pathway has predicted the following mechanism [7]:

$$CO_2 + e^- + H^+ + * \rightarrow COOH* \quad (1)$$

$$COOH* + H^+ + e^- \rightarrow H_2O + CO* \quad (2)$$

$$CO* \rightarrow CO + * \quad (3)$$

Adsorption of CO_2 or desorption of CO is the rate determining step.

Palladium-based electrocatalytic systems are found to be highly selective towards formate and carbon monoxide. Faradaic efficiency of the desired product can be increased by varying the applied potential and thereby the active site of the catalyst.[10]

Studies have shown that palladium exists as PdH_x in the reducing environment and has three possible phases α, β and a mixed phase $\alpha + \beta$ [8]. These phases correspond to random occupancy of octahedral voids of Pd FCC lattice by hydrogen atom. At room temperature ~70% of the octahedral voids are occupied [9]. The α phase is observed at $x < 0.017$ and the β phase is observed at $x > 0.58$ [8]. These phases exist in different potential regions (Figure 2) and affect the selectivity of the product thus formed.

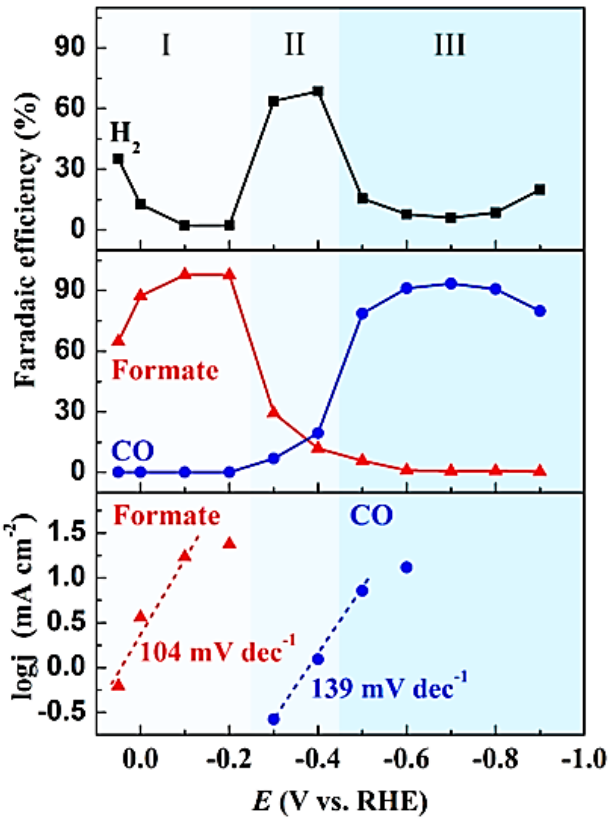

Figure 2: *Dependence of applied potential on faradaic efficiency of HCOOH, H_2, CO. (printed with permission from ref 10.)*

In the lower potential region i.e. < -0.2V (vs. RHE), α + β PdH_x exists [11, 10]. The surface is fully covered with hydrogen in this potential region. This phase reduces the CO_2 to formate via the HCOO* intermediate with high faradaic efficiency. In the -0.2 to -0.4 V region, an active phase transformation from the α + β PdH_x to the β PdH_x @Pd takes place. As a result the competitive HER reaction predominates wherein most of the surface PdH_x is destroyed by the adsorption of the CO* intermediate resulting in a partially H covered region. Desorption of CO becomes difficult because of its strong binding energy with the surface.[11, 10]

At higher potential, low coverage of hydrogen is observed and metallic palladium is the dominant phase on the surface. CO is formed through the intermediate COOH* which gets accumulated on the surface. This favors the formation of bulk PdH_x which weakens the CO* adsorbed on the surface [10, 12]. This results in high faradaic efficiency of carbon monoxide.

Theoretical calculations have shown that the edge (211) and the corner sites of palladium are catalytically more active for CO_2 reduction in comparison to the terrace (111) sites which are more active for the competing HER reaction [4, 13, 14]. Decreasing the nanoparticle size, would increase the density of the active sites i.e. more edge and corner sites would be exposed. The effect of particle size on faradaic efficiency was observed by D. Gao *et al*. [14] wherein they found that the faradaic efficiency of CO was 5.8% on 10.3 nm sized carbon supported Pd nanoparticles as the competing HER reactions was found to be dominant over the terrace sites. However, faradaic efficiency increased to 91.2 % over 3 nm sized Pd nanoparticles as the density of the edge and corner sites increased and CO_2 reduction became dominant. Similarly carbon supported Pd nanoparticles of 4nm size [4] showed a total faradaic efficiency of 80% for a mixture of CO and H_2. Thus it is important to synthesize well dispersed and smaller nanoparticles to obtain high faradaic efficiency.

An alternative carbon-based support extensively used for electrochemical reaction is graphitic carbon nitride. Graphitic carbon nitride is a semiconducting material. It consists of tri-s-triazine unit which are electrochemically active. Several morphologies of C_3N_4 have been studied for HER, OER, ORR and as supercapacitors [15, 16] Pd supported on C_3N_4 have been explored for hydrogen evolution reaction[17]. CO_2 electroreduction have been studied over Au nanoparticles supported on C_3N_4 [7]. The Faradaic efficiency of CO was found to be ~ 80% over this electrocatalyst. This was attributed to the donation of the unpaired electron on the nitrogen of the tri-s-triazine unit of C_3N_4 to the Au surface resulting in a negatively charged surface which facilitates the strong adsorption of the reaction intermediates and thereby enhancing the electrochemical activity.

3.2 Scope of the present study

Herein, efforts have been put to explore a new class of electrocatalysts based upon Pd-C_3N_4. This system has been chosen because C_3N_4 will act as an electrochemically active support due to the presence of triazine units. Furthermore, microwave-assisted synthesis and electrodeposition were used against the conventional techniques to synthesize well dispersed and nanosized Pd particles with high density of active sites to enhance the faradaic efficiency for CO.

3.3 Experimental Section:

3.3.1 Synthesis of g-C_3N_4

Graphitic carbon nitride was synthesized by a previously reported procedure [17]. In a typical synthesis, 5 g of melamine was taken in a crucible and heated under static air in a muffle furnace for 4 hrs at 550 ºC at 2.3 ºC/min ramp rate. Obtained C_3N_4 was used as such for further synthesis of Pd@C_3N_4.

3.3.2 Microwave assisted synthesis of Pd@C_3N_4 -MW

The catalyst was synthesized by modifying previously reported procedure [18, 19]. In a typical synthesis, 50 mg of C_3N_4 was dispersed in a 20 mL mixture of isopropyl alcohol and water (1:3). The resultant dispersion was probe sonicated for 30 mins to exfoliate C_3N_4. A 6.1 μL of 0.1 M H_2PdCl_4 (equivalent to 5 wt% Pd) was added to the above dispersion and stirred overnight. A 5ml of resultant mixture was placed in a microwave reactor. The reactor was set for a heating-cooling cycle between 80 ° C and 60 ° C respectively with 20 repetitions under a constant power of 100 W. The solution obtained post microwave treatment was centrifuged and the supernatant was collected.

3.3.3 Electrodeposition of Pd on C_3N_4 (Pd@C_3N_4 – ED)

Electrodeposition was carried out in a three electrode electrochemical cell (as shown in figure 3). Carbon paper coated with C_3N_4 was used as the working electrode, graphite electrode as the counter electrode and Ag/AgCl electrode as the reference electrode. The electrodes were dipped in a 12 ml solution of 0.1 M HCl and 0.1 mM K_2PdCl_4. Electrodeposition was performed by applying -0.241V potential for 20 seconds. The electrodeposited carbon paper was washed with MilliQ water to remove any unreacted Pd on the surface. The electrodeposited electrode was further used for CO_2 electroreduction studies.

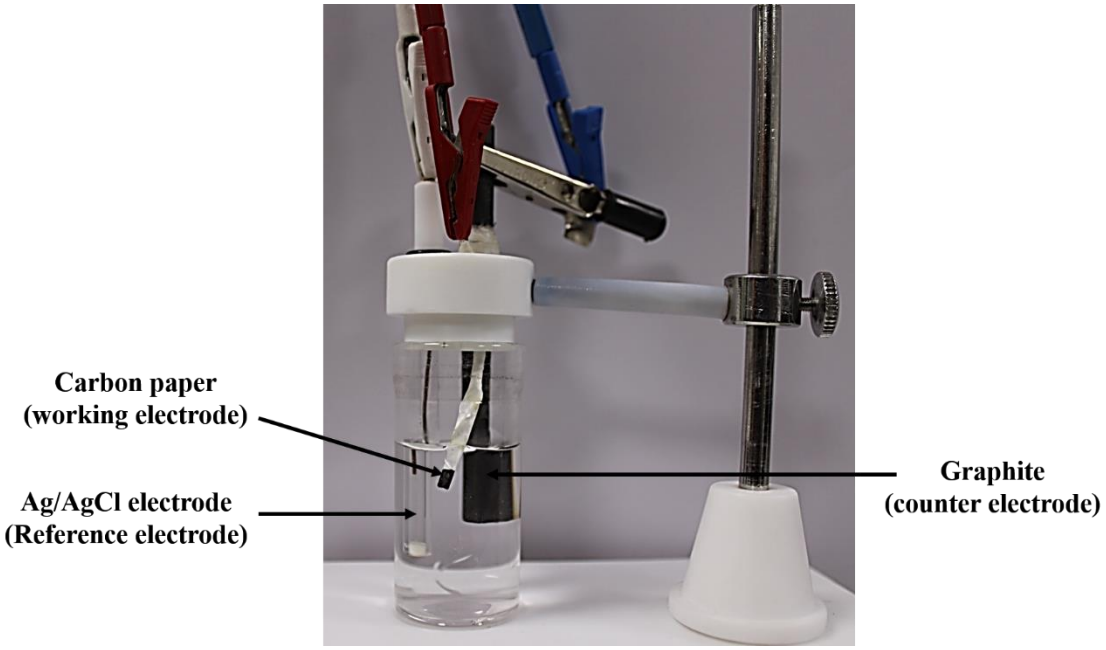

Figure 3: *Electrochemical setup for electrodeposition.*

3.3.4 p-Nitrophenol reduction

Reduction of p-Nitrophenol is a model reaction to test the catalytic activity of a catalyst. This reduction reaction was thus used to test the catalytic activity of the catalyst prepared by microwave assisted synthesis. In a typical procedure, 2ml of 100 μM p-nitrophenol was taken in a quartz cuvette. To this, 1 ml of 10 mM sodium borohydride solution ($NaBH_4$) was added resulting in the appearance of bright yellow color. The UV-Visible spectra was recorded for the solution. 0.1 ml of the as synthesized catalyst was added to the above solution and the UV-Visible spectra was recorded at every 2 mins time interval.

Time dependence spectra was obtained by recording the change in intensity of the absorbance peak at 400 nm at every 15 sec. Similarly, temperature dependence study was performed by recording the change in intensity of the absorbance peak at 400 nm at every 5 secs at the desired temperature.

3.3.5 Preparation of electrodes

1 mL solution of the supernatant obtained from microwave-assisted synthesis of Pd@C_3N_4-MW was taken in a vial. To this 20 μL Nafion (binder) was added. The resultant mixture was sonicated for 1 hour. 0.5 ml of the coating ink thus prepared was

coated onto a carbon paper of dimension 0.5 × 0.5 cm. The electrode prepared was washed thoroughly with Milli Q water to remove any unreacted K_2PdCl_4.

3.3.6 CO_2 electroreduction

The electrochemical measurements were carried out in an H-type cell consisting of a three electrode system. Carbon paper coated with the catalyst was used as the working electrode. Ag/AgCl and Pt was used as the reference and counter electrode respectively. The anodic and the cathodic chamber contained 20 ml of 0.5 M $KHCO_3$ each. The two chambers were separated by a Nafion membrane. The 20 ml, 0.5 M $KHCO_3$ present in the cathodic chamber was bubbled with CO_2 for 30 mins before the linear sweep voltammetric measurement. Further, to analyze the products obtained, chronoamperometric studies were carried out at -1.5 V reduction potential for 40 mins.

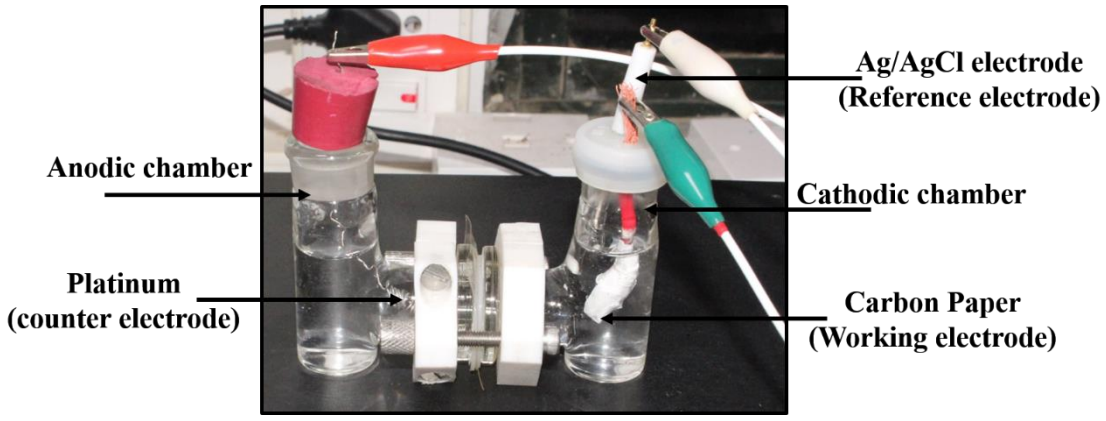

Figure 4: *H-type cell used to study the electrochemical reduction of CO_2*

3.4 Sample Characterisations:

Powder X-Ray Diffraction measurements were recorded using Rigaku using Cu Kα radiations. The morphologies of the sample was examined using Field Emission scanning electron microscopy ZEISS Gemini 500 FESEM and FESEM FEI Nova-Nano SEM-600. The elemental composition was determined by Energy Dispersive X-Ray Scattering technique using ZEISS Gemini 500 FESEM and Tecnai, T20. The transmission electron microscopy images were obtained using JEOL JEM-3010 at 300 kV and Tecnai, T20 at 200 kV. The UV-Vis absorbance spectra was recorded using Perkin Elmer Lambda 900 UV-Vis-NIR spectrometer. Electrochemical measurements

were done using Biologic, EC Lab. The products obtained were analyzed using gas chromatography, Perkin Elmer, Clarus 580 GC equipped with TCD and FID.

3.5 Results and Discussion:

3.5.1 Characterisations

The PXRD pattern of C_3N_4 synthesized by polycondensation of is shown in figure 5.

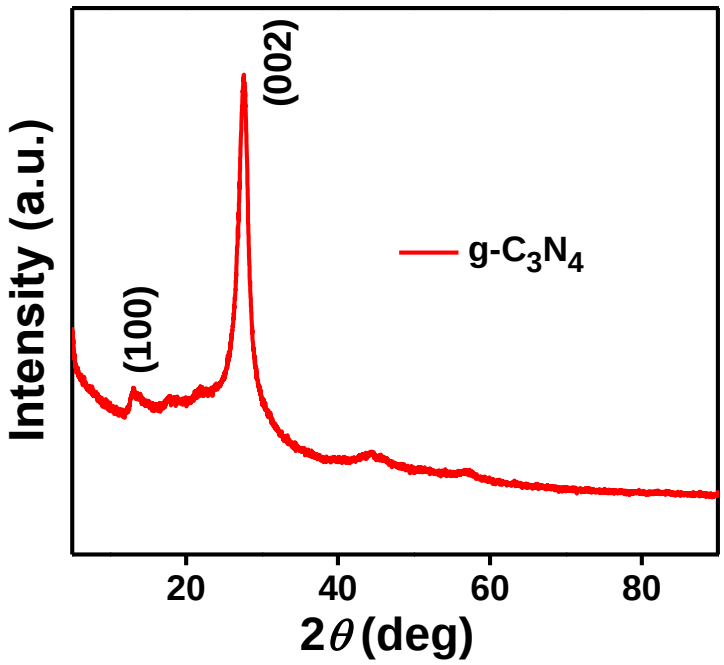

Figure 5: *Powder X-Ray Diffraction pattern of g-C_3N_4*

The characteristic peaks at 2θ = 13.1 corresponding to (100) [20] plane of g-C_3N_4 and also at 27.5 degrees corresponding to (002) [20] plane. The peak at 2θ = 13.1 correspond to intralayer d- spacing of 0.69 nm [20]. While peak at 2θ = 27.5 degrees corresponds to interlayer d-spacing of 0.326 nm [20].

The presence of Pd nanoparticles in the supernatant obtained from microwave assisted synthesis was confirmed by energy dispersive X-ray scattering (EDS) analysis which showed Pd loading over C_3N_4 support. Further, the TEM analysis of the supernatant (Figure 4) showed uniformly dispersed Pd nanoparticles over C_3N_4. The average particle size of 2 nm as obtained from particle size distribution histogram counted over 81 particles.

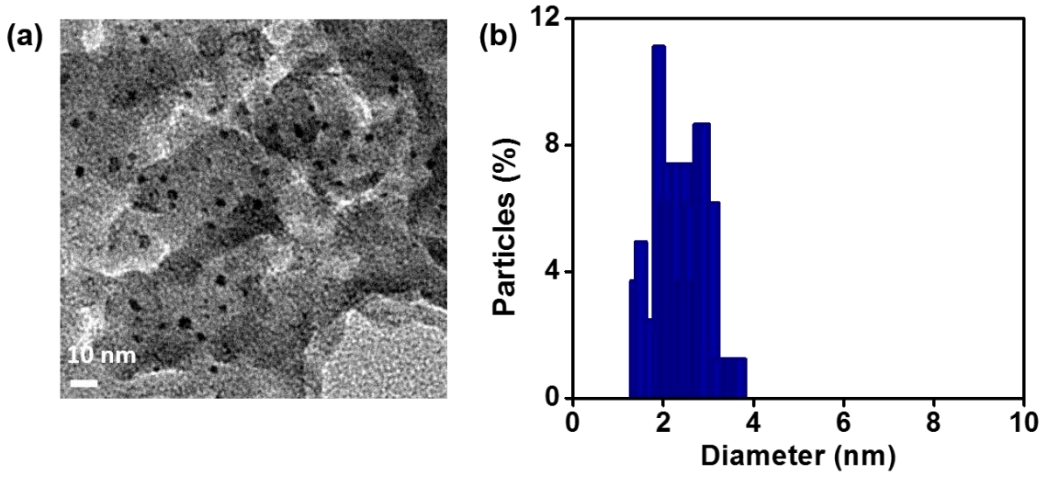

Figure 6: (a) *Transmission Electron Microscopy image of Pd nanoparticles dispersed over g-C_3N_4* **(b)** *Histogram of size distribution of the particles (counted over 81 particles)*

The supernatant obtained from microwave synthesis was coated onto a carbon paper which was then used as a working electrode for CO_2 electroreduction. The elemental mapping and EDS analysis was performed to gain a qualitative insight in to the changes occurring in the elemental composition of the carbon paper loaded with electrocatalyst during the electrochemical CO_2 reduction reaction.

The elemental mapping of the the carbon paper coated with 5 wt% Pd over 5 mg C_3N_4 taken before CO_2 electroreduction reaction (Figure 7) showed the presence of Pd, K and N on the carbon support. Further EDS analysis showed 89 wt% of N, 7 wt% of Pd and 4 wt% of K on the carbon support. The elemental mapping of the the carbon paper coated with 5% Pd over 5 mg C_3N_4 taken after CO_2 electroreduction reaction (Figure 8) shows the presence of Pd, K and N on the carbon support. The elemental composition of the carbon paper was determined by EDS analysis showed the presence of 52 wt% of N, 42 wt% of K and 5 wt% Pd on the carbon paper. Enhanced presence of K may be attributed to the intercalation of potassium ions into the carbon paper [23] during the reaction since it is performed under high negative potential conditions and in $KHCO_3$ electrolytic medium .

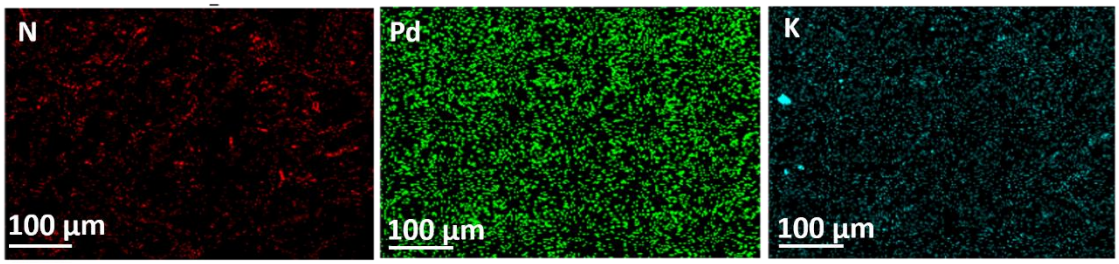

Figure 7: *Elemental Mapping of the carbon paper coated with 5% Pd over 5 mg C_3N_4 (Pd-C_3N_4-MW) taken before CO_2 electroreduction reaction.*

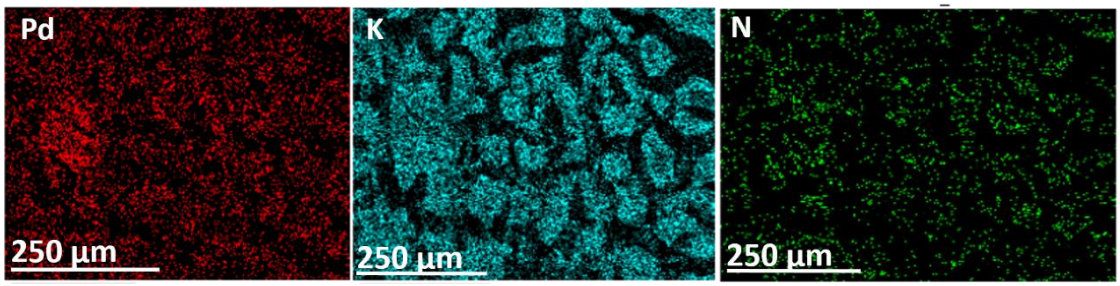

Figure 8: *Elemental Mapping of the carbon paper coated with 5% Pd over 5 mg C_3N_4 (Pd-C_3N_4-MW) taken after CO_2 electroreduction reaction.*

The Pd-C_3N_4 prepared by electrodeposition was characterised by FESEM and EDS. The FESEM image of the carbon paper coated with g- C_3N_4 followed by electrodeposition of Pd shows uniform deposition of spherical Pd particles over the carbon fibres. The particles are found to be in 200-250 nm range. The high Z-contrast between the particles and carbon fibre may be attributed to the significant backscattering by the metal particles which makes it appear brighter.

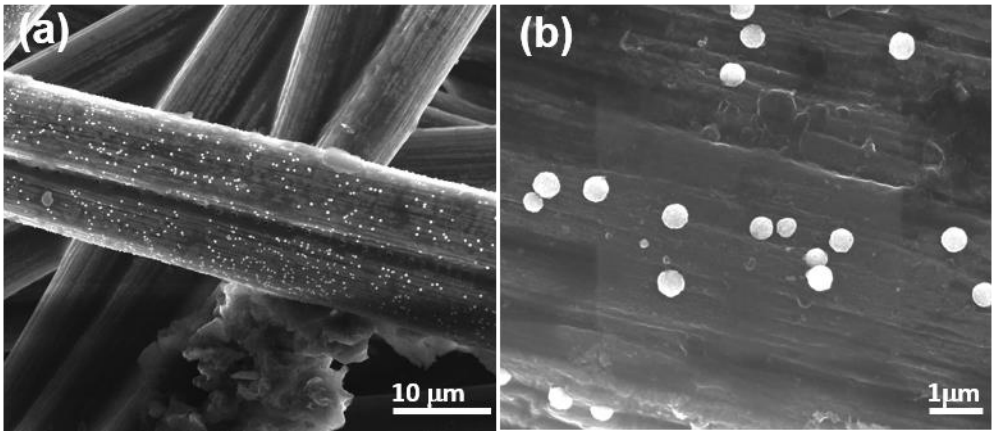

Figure 9: *FESEM images of the carbon paper coated with C_3N_4 post electrodeposition of Pd under* **(a)** *low magnification and* **(b)** *high magnification.*

EDS analysis further confirmed the presence of Pd particles wherein Pd loading was found to be 5 wt%. However, exact loading of Pd particles need to be determined by ICP analysis.

3.5.2 Catalyst activity

3.5.2.1 p-Nitrophenol reduction

The catalytic activity of Pd on C_3N_4 prepared by microwave (Pd-C_3N_4-MW) assisted synthesis was estimated using borohydride reduction of p- nitrophenol to aminophenol as a test reaction. p-Nitrophenol is reduced to aminophenol in the presence of excess BH_4^- ion and catalyst making it a pseudo first order reaction. The reaction proceeds via the Langmuir-Hinshelwood Mechanism wherein, the reactants i.e., p-nitrophenol and BH_4^- gets adsorbed on the catalyst surface for the reduction to take place. Upon addition of $NaBH_4$, characteristic peak corresponding to nitrophenolate ion appear at 400 nm.

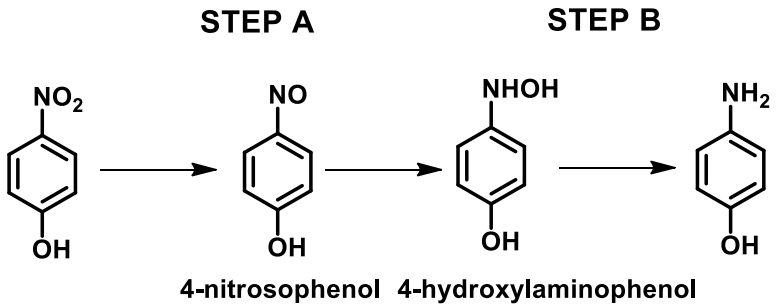

Scheme 1: (a) *Mechanistic pathway for p-nitrophenol reduction. (printed with permission from ref.21)*

The reaction proceeds by the mechanism shown in scheme 1 wherein two intermediates namely, 4-nitrosophenol and 4-hydroxyaminophenol are formed during the course of the reaction. Out of these, 4-hydroxyaminophenol is the most stable intermediate. Consequently, step B shown in scheme 1 is a slow step and hence, it is the rate determining step. The reactants and the intermediates binds to the active site of the catalyst during the reaction. 4-hydroxyaminophenol gets adsorbed strongly to the active site, which slows down the reaction. The reduction reaction can be monitored by UV-visible spectroscopy. As the reaction proceeds, the intensity of absorbance at 400 nm decreases and a peak at 316 nm corresponding to aminophenol appears.

In the present study, p-nitrophenol reduction by Pd on C_3N_4 prepared by microwave assisted synthesis was tested. In the absence of the catalyst nitrophenol reduction was not observed. However, upon addition of catalyst significant increase in the rate of reduction reaction was observed.

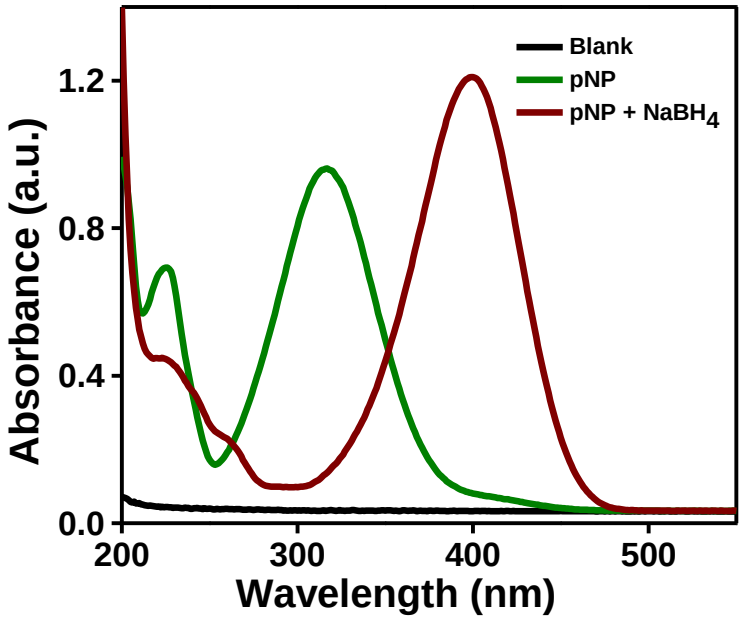

Figure10: (a) *Absorbance spectra of p-Nitrophenol before and after addition of $NaBH_4$*

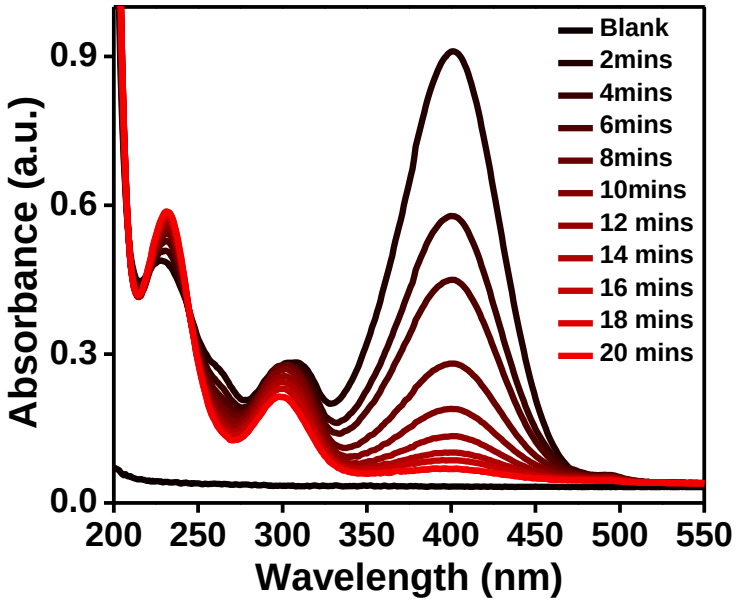

Figure10: (b) *Reduction of p-Nitrophenol upon addition of Pd-C_3N_4-MW (5% Pd dispersed on C_3N_4 prepared by microwave synthesis).*

As discussed earlier, formation of nitrophenolate ion results in the absorbance peak at 400 nm (Figure 10a). The progress of the reaction is evident from the decrease in the intensity of the absorbance peak at 400 nm and simultaneous appearance of the characteristic absorbance peak at 316 nm of aminophenol (Figure 10b).

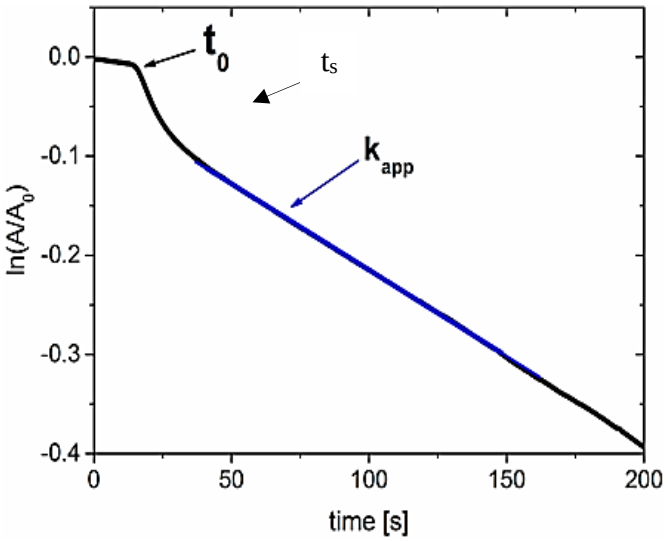

Figure 11: *Time dependence plot of change in absorption of p-nitrophenolate ion at 400 nm. (printed with permission from Ref 21.)*

Study of the reduction reaction as a function of time, helps in determining the rate constant. As shown in Figure 11, the time dependence curve has two regions. Region 1 correspond to the induction period during which the active site of the catalyst rearrange themselves or in other words, surface restructuring takes place. This is followed by region 2 known as the stationary state, during which the reduction reaction take place. The rate constant is calculated using equation 1:

$$\ln \frac{A(t)}{A(o)} = ln \frac{C(t)}{C(o)} = -k_{app}\, t_s$$

Wherein, A(t) = absorbance at time t, A_o = absorbance at t_o, C(t)=concentration of nitrophenol at time t, C_o= concentration of nitrophenol at t_o, K_{app}= apparent rate constant and t_s = time at which stationary state begins

Further, Arrehnius plot is used to determine the activation energy of the reaction. It is a plot of ln k vs 1/T. the slope of the curve can be used to calculate the activation energy using equation 2:

$$lnk = lnA - \frac{Ea}{RT}$$

Where, k = rate constant at temperature T, A= Arrehnius constant, E_a = activation energy, R= universal gas constant and T = temperature.

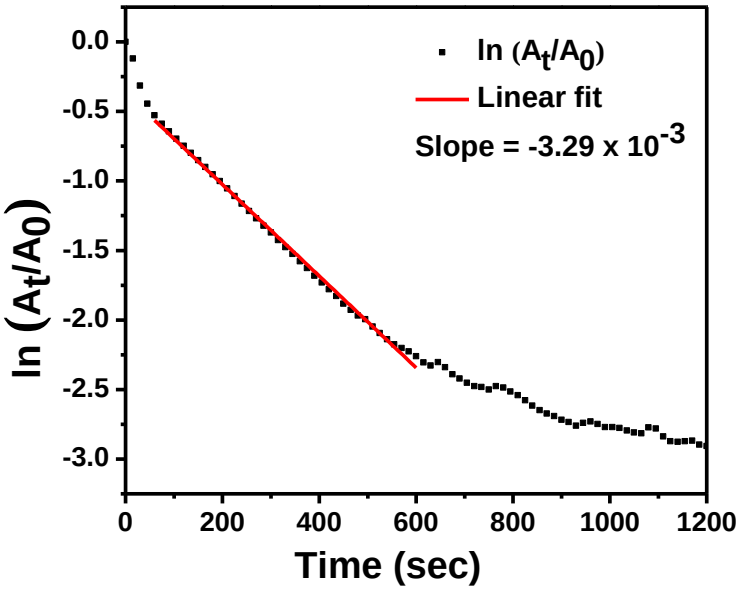

Figure 12: (a) *Reduction of p-Nitrophenol in the presence of Pd-C_3N_4-MW shows decreasing absorbance at 400 nm over a period of 20 mins, readings taken at 15s*

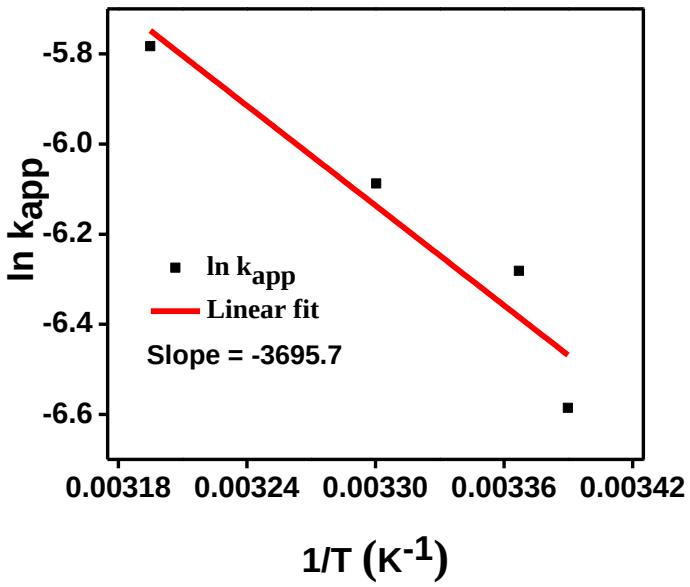

Figure 12: (b) *Arrehenius plot to determine the activation energy for reduction of p-Nitrophenol.*

Reduction of p-nitrophenol was studied over a period of 20 mins. The decrease in intensity of the absorbance peak at 400 nm was studied. The rate constant was calculated using equation 1 and was found to be 3.29 x 10^{-3} s^{-1}. This value was found to be lower than the previously reported rate constant value (11 x 10^{-3} s^{-1}) for Pd supported on C_3N_4 [17]. The activation energy for the reaction was determined using equation 2 and was found to be 30.73 kJ/mol.

3.5.2.2 Electrochemical CO_2 reduction studies

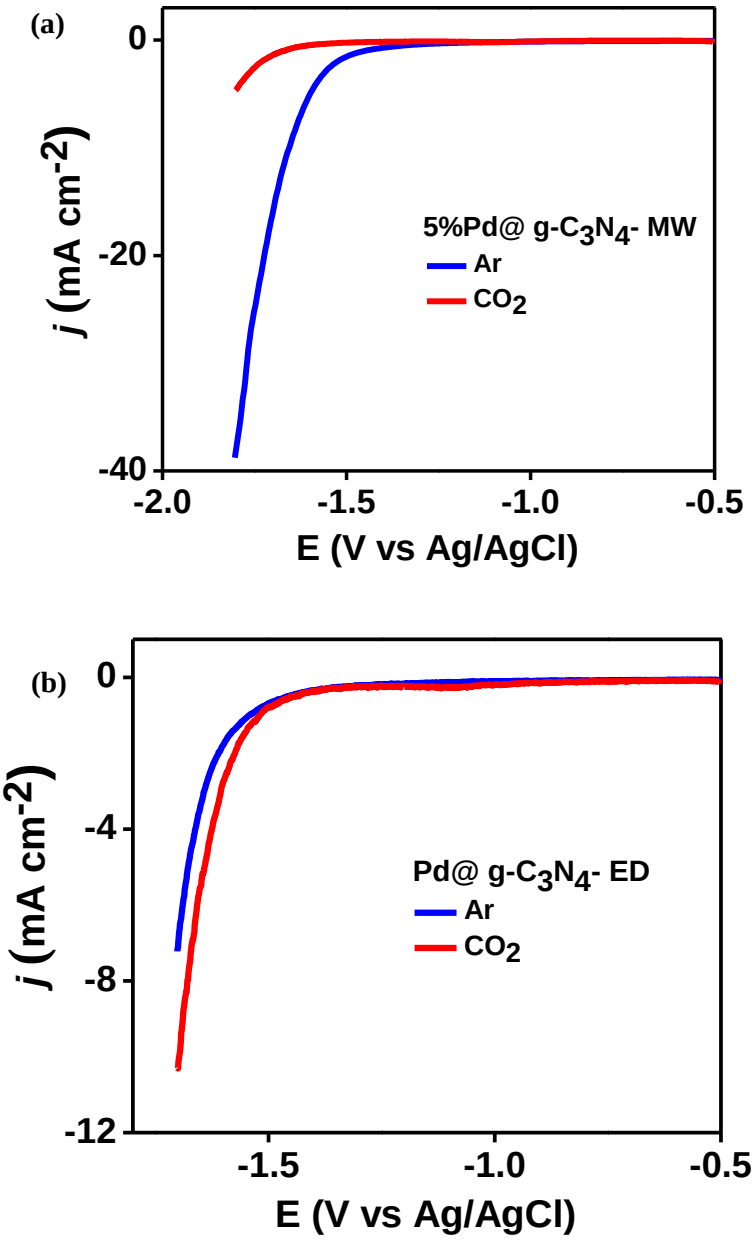

Figure 13: *Linear sweep voltammograms in both Ar and CO_2 saturated 0.5 M $KHCO_3$ solution for* ***(a)*** *Pd@C_3N_4-MW* ***(b)*** *Pd@C_3N_4 –ED.*

Current density acts as an essential marker to study the kinetics of the electrochemical reaction. Higher current density results in a higher charge transfer. This leads to an efficient electrochemical process. Figure 13a shows the linear sweep voltammograms recorded under Ar and CO_2 saturated atmosphere in the presence of Pd@C_3N_4 –MW. It can be observed that the current density under the Ar saturated atmosphere is higher. This may be attributed to the hydrogen evolution reaction that takes place in the reducing environment. However, in a CO_2 saturated atmosphere, both HER and CO_2 electroreduction takes place. The intermediated formed during the reduction reaction compete for the active site of the catalyst. In the present case, CO_2 electroreduction seems to be the dominant reaction resulting in a low current density value. The low current density value may be attributed to the thermodynamic stability of the CO_2. As a result the reaction takes place at a higher negative potential compared to HER and at a different rate.

Figure 13b shows the linear sweep voltammograms recorded under Ar and CO_2 saturated atmosphere in the presence of Pd@C_3N_4 –ED. It can be observed that the voltammograms corresponding to only HER in the argon saturated atmosphere and the competing reactions in the CO_2 saturated atmospheres are comparable. This may be attributed to the comparable rates of HER and CO_2 electroreduction reaction.

Further, potentiostatic measurements were performed for 40 mins at -1.5 V to get the products of electrochemical reduction. Gas chromatography analysis using a GC equipped with FID and TCD yielded H_2 and CO as the major product and methane as the minor product. CO obtained upon using Pd@C_3N_4 –MW is higher. One of the possible reason for this activity could be the small size of the Pd particles obtained by microwave assisted synthesis. The small sized particles result in increased density of exposed edge and corner sites of Pd particles which are found to be highly active for CO_2 reduction reaction [12]. The large sized particles obtained by electrodeposition decreases the density of the edge and the corner sites [12]. This results in dominant HER reaction and thereby the major product obtained in this case is hydrogen and CO is the minor product.

3.6 Conclusions

In the present study, Pd supported on C_3N_4 have been synthesized by electrodeposition and by microwave assisted synthesis. Pd particles obtained by microwave assisted

synthesis were found to be ~2 nm sized. While, the Pd particles obtained by electrodeposition were found to be in 200-250 μm regime. The major products obtained by CO_2 reduction reaction was found to be H_2 and CO. CO was the major product obtained in the former case and H_2 was the major product obtained in the latter case.

3.7 Future Directions

Electrodeposition is a fast method to synthesize an electrocatalyst with small size an desired morphology. Hence, further optimisations for decreasing the particle size and thereby increasing the catalytic activity would be performed. Characterizations to determine the exact nature of the active sites responsible for CO_2 reduction will be carried out. To determine the exact loading of Pd, ICP analysis have to be done. Further optimizations to determine the Faradaic efficiency of the product obtained have to be performed. Studies to determine the role of C_3N_4 have to be conducted.

3.8 References

(1) https://www.statista.com/chart/15737/global-co2-emissions-ipcc-targets/

(2) http://www.oica.net/category/climate-change-and-co2/

(3) Zhang, W.; Hu, Y.; Ma, L.; Zhu, G.; Wang, Y.; Xue, X.; Chen, R.; Yang, S.; Jin, Z. Progress and Perspective of Electrocatalytic CO_2 Reduction for Renewable Carbonaceous Fuels and Chemicals. *Adv. Sci.* **2018**, *5* (1).

(4) Sheng, W.; Kattel, S.; Yao, S.; Yan, B.; Liang, Z.; Hawxhurst, C. J.; Wu, Q.; Chen, J. G. Electrochemical Reduction of CO_2 to Synthesis Gas with Controlled CO/H_2 Ratios. *Energy Environ. Sci.* **2017**, *10* (5), 1180–1185.

(5) Chen, P.; Jiao, Y.; Zhu, Y.; Chen, S.; Song, L.; Jaroniec, M.; Zheng, Y.; Qiao, S. Syngas Production from Electrocatalytic CO_2 Reduction with High Energetic Efficiency and Current Density. *J. Mater. Chem. A* **2019**.

(6) Hori, Y.; Tsukamoto, T.; Koga, O. Process of CO Selectivity in Electrochemical Reduction of CO_2 at Metal Electrodes in Aqueous Media. *Electrochim. Acta* **1994**, *39*, 1833–1839.

(7) Wang, H. F.; Zheng, L. R.; Mao, F.; Zhang, L.; Yang, X. H.; Yang, H. G. Tuning Metal Catalyst with Metal–C 3 N 4 Interaction for Efficient CO_2 Electroreduction *ACS Catal.* **2018**, *8* (12), 11035–11041.

(8) Manchester, F. D.; San-Martin, A.; Pitre, J. M. The H-Pd (Hydrogen-Palladium) System. *J. Phase Equilibria* **1994**, *15* (1), 62–83.

(9) Greenwood. *Chemistry of the Elements*; Elsevier Science & Technology Books, 1996.

(10) Gao, D.; Zhou, H.; Cai, F.; Wang, D.; Hu, Y.; Jiang, B.; Cai, W. Bin; Chen, X.; Si, R.; Yang, F.; et al. Switchable CO2 Electroreduction via Engineering Active Phases of Pd Nanoparticles. *Nano Res.* **2017**, *10* (6), 2181–2191.

(11) Gao, D.; Zhou, H.; Cai, F.; Wang, J.; Wang, G.; Bao, X. Pd-Containing Nanostructures for Electrochemical CO2 Reduction Reaction. *ACS Catal.* **2018**, *8* (2), 1510–1519.

(12) Dai, Y.; Mu, X.; Tan, Y.; Lin, K.; Yang, Z.; Zheng, N.; Fu, G. Carbon Monoxide-Assisted Synthesis of Single-Crystalline Pd Tetrapod Nanocrystals through Hydride Formation. *J. Am. Chem. Soc.* **2012**, *134* (16), 7073–7080.

(13) Jiang, B.; Zhang, X. G.; Jiang, K.; Wu, D. Y.; Cai, W. Bin. Boosting Formate Production in Electrocatalytic CO_2 Reduction over Wide Potential Window on Pd Surfaces. *J. Am. Chem. Soc.* **2018**, *140* (8), 2880–2889.

(14) Gao, D.; Zhou, H.; Wang, J.; Miao, S.; Yang, F.; Wang, G.; Wang, J.; Bao, X. Size-Dependent Electrocatalytic Reduction of CO_2 over Pd Nanoparticles. *J. Am. Chem. Soc.* **2015**, *137* (13), 4288–4291.

(15) Niu, W.; Yang, Y. Graphitic Carbon Nitride for Electrochemical Energy Conversion and Storage. *ACS Energy Lett.* **2018**, *3* (11), 2796–2815.

(16) Niu, P.; Zhang, L.; Liu, G.; Cheng, H. M. Graphene-like Carbon Nitride Nanosheets for Improved Photocatalytic Activities. *Adv. Funct. Mater.* **2012**, *22* (22), 4763–4770.

(17) Nazir, R.; Fageria, P.; Basu, M.; Gangopadhyay, S.; Pande, S. Decoration of Pd and Pt Nanoparticles on a Carbon Nitride (C3N4) Surface for Nitro-Compounds

Reduction and Hydrogen Evolution Reaction. *New J. Chem.* **2017**, *41* (18), 9658–9667.

(18) Midgley, P. A.; Ortuño, M. A.; Collins, S. M.; López, N.; Vorobyeva, E.; Fako, E.; Pérez-Ramírez, J.; Mitchell, S.; Vilé, G.; Richard, S.; Chen, Z. A Heterogeneous Single-Atom Palladium Catalyst Surpassing Homogeneous Systems for Suzuki Coupling. *Nat. Nanotechnol.* **2018**, *13* (8), 702–707.

(19) Wang, X.; Zhan, L.; Ajayan, P. M.; Zhang, J.; Yang, S.; Fang, Z.; Gong, Y.; Vajtai, R.; Ma, L. Exfoliated Graphitic Carbon Nitride Nanosheets as Efficient Catalysts for Hydrogen Evolution Under Visible Light. *Adv. Mater.* **2013**, *25* (17), 2452–2456.

(20) Fina, F.; Callear, S. K.; Carins, G. M.; Irvine, J. T. S. Structural Investigation of Graphitic Carbon Nitride via XRD and Neutron Diffraction. *Chem. Mater.* **2015**, *27* (7), 2612–2618.

(21) Gu, S.; Wunder, S.; Lu, Y.; Ballau, M.; Fenger, R.; Rademann, K. Kinetic Analysis of the Catalytic Reduction of 4 - Nitrophenol by Metallic Nanoparticles. *J. Phys. Chem. B* **2014**, *118*, 18618–18625.

(22) Zhi, X.; Jiao, Y.; Zheng, Y.; Qiao, S. Impact of Interfacial Electron Transfer on Electrochemical CO 2 Reduction on Graphitic Carbon Nitride / Doped Graphene. *Small* **2019**, *1804224*, 1–7.

(23) Acerce, M.; Voiry, D.; Chhowalla, M. Metallic 1T Phase MoS_2 Nanosheets as Supercapacitor Electrode Materials. *Nat. Nanotechnol.* **2015**, *10*, 313.

(24) Zhao, Z.-J.; Yang, P.; Zhu, W.; Gong, J.; Chang, X.; Hu, C.; Luo, Z.; Zhang, L. Low-Coordinated Edge Sites on Ultrathin Palladium Nanosheets Boost Carbon Dioxide Electroreduction Performance. *Angew. Chemie Int. Ed.* **2018**, *57* (36), 11544–11548.

(25) Min, X.; Kanan, M. W. Pd-Catalyzed Electrohydrogenation of Carbon Dioxide to Formate: High Mass Activity at Low Overpotential and Identification of the Deactivation Pathway. *J. Am. Chem. Soc.* **2015**, *137* (14), 4701–4708.

(26) Mohanty, U. S. Electrodeposition: A Versatile and Inexpensive Tool for the Synthesis of Nanoparticles, Nanorods, Nanowires, and Nanoclusters of Metals. *J. Appl. Electrochem.* **2011**, *41* (3), 257–270.

(27) Pan, Y.; Lin, R.; Chen, Y.; Liu, S.; Zhu, W.; Cao, X.; Chen, W.; Wu, K.; Cheong, W. C.; Wang, Y.; et al. Design of Single-Atom Co-N5Catalytic Site: A Robust Electrocatalyst for CO2Reduction with Nearly 100% CO Selectivity and Remarkable Stability. *J. Am. Chem. Soc.* **2018**, *140* (12), 4218–4221.

(28) Feng, D.-M.; Zhu, Y.-P.; Chen, P.; Ma, T.-Y. Recent Advances in Transition-Metal-Mediated Electrocatalytic CO2 Reduction: From Homogeneous to Heterogeneous Systems. *Catalysts* **2017**, *7* (12), 373.